Cement and Concrete Research 198 (2025) 107983

Contents lists available at ScienceDirect

Cement and Concrete Research

journal homepage: www.elsevier.com/locate/cemconres

Basic oxygen furnace (BOF) slag cementitious binder activated by Na_4EDTA

Zhihan Jiang [a], Xuan Ling [a,*], Quan Liu [a], Helong Song [b], Katrin Schollbach [a], H.J.H. Brouwers [a]

[a] Department of the Built Environment, Eindhoven University of Technology, Eindhoven 5600 MB, the Netherlands
[b] College of Civil and Transportation Engineering, Shenzhen University, Shenzhen 518060, China

ARTICLE INFO

Keywords:
BOF slag binder
Tetrasodium EDTA (Na_4EDTA)
Chelation-promoted hydration
Mineral phase evolution
Leaching

ABSTRACT

Basic oxygen furnace (BOF) slag contains two potentially hydraulically reactive phases, belite (C_2S) and brownmillerite ($C_2(A,F)$), yet exhibits low reactivity. This study proposes ethylenediaminetetraacetic acid tetrasodium salt (Na_4EDTA) as a hydration activator and investigates its effects on BOF slag phase evolution, early hydration kinetics, microstructural development, mechanical properties, and leaching behaviors. The $EDTA^{4-}$ chelation mechanism in the BOF slag system is also discussed. Results show that Na_4EDTA significantly enhances BOF slag hydration, producing a stand-alone binder with high compressive strength (38.8 MPa at 28 d, v.s. 8.6 MPa of the reference) and reduced porosity. At 4.8 wt% Na_4EDTA, brownmillerite reacts almost completely within one day. Belite hydration is also enhanced, particularly at early ages. The main hydration products are hydrogarnet and C-S-H gel. EDTA itself is likely partially incorporated into the layered double hydroxides (LDHs) structure of hydrotalcite. Heavy metal leaching is below the Dutch legal limits.

1. Introduction

BOF slag is a solid waste (by-product) generated during the basic oxygen furnace (Linz–Donawitz) steelmaking process formed by the reaction of the fluxes with the impurities in the hot metal and the scrap [1]. In this process, molten pig iron and steel scraps are transformed into steel by blowing oxygen and adding fluxes [2]. Lime and dolomite are added to the furnace as fluxes to remove impurities such as phosphorus and sulfur and protect the lining [3]. The global production of BOF slag is estimated to be about 200 million tons annually, accounting for about 60 % of the total steel slag output [4]. Typical main minerals present in BOF slag are dicalcium silicate (C_2S), brownmillerite ($C_2(A,F)$), magnetite (Fe_3O_4), FeO-MgO-MnO solid solution (RO phase) in the wuestite structure, and free lime (CaO), as well as possible small amounts of tricalcium silicate (C_3S) [2,5–7]. The general chemical constituents of BOF slag are CaO (40–60 %), Fe_2O_3 (20–40 %), SiO_2 (10–20 %), MgO (2–10 %), Al_2O_3 (1–7 %), and MnO (0–4 %), with minor amounts of P_2O_5, V_2O_5, Cr_2O_3, and TiO_2 [2,8,9].

The colossal generation and accumulation of BOF slag can cause numerous environmental problems, such as land waste and potential soil or water pollution due to the leaching of potentially toxic heavy metals, especially V and Cr [10–13]. From another point of view, the cement industry consumes too much energy and mineral resources while releasing greenhouse gases (CO_2 mainly) and other pollutants [14,15]. Using BOF slag as a stand-alone alternative cementitious material can efficiently consume and utilize BOF slag and alleviate problems caused by cement manufacturing. The similar mineral composition to cement, more specifically, the high content of potentially hydraulically active phases, brownmillerite and C_2S, within BOF slag, provides the possibility for this application [1,2,16,17]. However, the C_2S (mainly present as α' and β polymorphs) within BOF slag has limited reactivity, especially in early ages [2,8,10,16]. The brownmillerite in BOF slag also tends to be much less reactive than in OPC [8,10,18]. Thus, BOF slag needs to be adequately activated prior to being used as a stand-alone cementitious material. The hydration and activation of BOF slag have aroused great interest in academia, and many activation methods have been investigated, such as thermal and mechanical activation, using chemical activators (common alkalis, salts, and emerging ligands) [5,8,11,14,17–25].

In order to significantly improve the reactivity of BOF slag for widespread use as a stand-alone cement-free binder, it is necessary to start from the root cause of its poor hydration performance. As mentioned above, despite the abundant presence of C_2S ($\alpha' + \beta$), its intrinsic reactivity is relatively low, especially compared with the C_3S that is the main component of OPC. Hydration is further hindered by impurities (primarily P^{5+}, V^{5+}, and Fe^{3+}) [26,27]. In addition to C_2S, abundant brownmillerite ($C_2(A,F)$) (up to 18 wt%, as characterized in previous research [8,10]) is another potentially hydraulically active phase within BOF slag. Unlike C_2S, which mainly contributes to late

* Corresponding author.
E-mail address: x.ling@tue.nl (X. Ling).

https://doi.org/10.1016/j.cemconres.2025.107983
Received 17 March 2025; Received in revised form 29 May 2025; Accepted 4 July 2025
Available online 11 July 2025

strength development (after 28 days in Portland cement), brownmillerite (ferrite) quickly dissolves and hydrates when initially in contact with water in OPC [28,29]. However, the reactivity of brownmillerite (ferrite) containing large amounts of Fe is very low [8,10]. Additionally, the non-neglectable incorporation of Ti (around 5 wt% of brownmillerite) also hinders the hydration capacity of brownmillerite [8,10,30]. As discussed previously, several ligands have been explored to overcome the inherently low reactivity of BOF slag by virtue of their complexation abilities. Notable examples include tripotassium citrate, sodium oxalate, ethyl diisopropylamine (EDIPA), triethanolamine (TEA), triisopropanolamine (TIPA), diethanol isopropanolamine (DEIPA) and methyl diethanolamine (MDEA) [8,11,14,31–34]. They all significantly enhance BOF (steel) slag hydration (dissolution). In this research, we introduce Na_4EDTA as a novel activator, motivated by its hexadentate coordination geometry and superior chelation capacity compared to the aforementioned ligands, as characterized by the high stability constants of metal-EDTA complexes [35–41]. Furthermore, ethylenediaminetetraacetic acid (EDTA) and corresponding salts are some of the most important industrial chelators (ligands) that are produced at a massive scale and widely used in water treatment, cleaning agents, cosmetics and personal care products, the food industry, and the pharmaceutical industry [41–45]. Within the building materials field, the effects of EDTA or disodium EDTA on OPC, magnesium oxysulfate cement, and calcium sulphoaluminate-belite cement have been investigated [46–48]. Na_4EDTA is the fully deprotonated tetrasodium salt form of EDTA, which has the highest chelation power of the EDTA series and is expected to improve the hydration performance of BOF slag by promoting the dissolution of potentially hydraulically reactive phases, brownmillerite and C_2S ($\alpha' + \beta$), through fast adsorption, lone electron pairs transferring, and resulting crystal lattice disrupting process [47–51]. Thus, a stand-alone BOF slag binder based on Na_4EDTA activation is first proposed in the research. Varying doses of Na_4EDTA are utilized, and their effects on BOF slag hydration kinetics, phase composition evolution, mechanical strength, and pore properties are investigated thoroughly. Multiple techniques, including isothermal calorimetry, quantitative X-ray diffraction (XRD) and thermogravimetric (TG) analysis, compressive strength tests, mercury intrusion porosimetry (MIP) tests, fourier transform infrared spectroscopy (FTIR) spectroscopy are applied in the process. To evaluate the leaching possibility of BOF slag binder with the activation of Na_4EDTA, the one-stage leaching test is performed, and the leached ionic concentrations are obtained based on the inductively coupled plasma atomic emission spectrometer (ICP-AES, SPECTROBLUE). Finally, the complexation mechanism of metal-EDTA is discussed, and the possible $EDTA^{4-}$ ($[M\text{-}EDTA]^{n-}$ complexes) incorporation model (into the hydration product matrix), EDTA-embedded hydrotalcite LDHs, is proposed.

2. Materials, specimens, and methods

2.1. Raw materials and the activator

The BOF slag used in this research was collected from the standard production line of Tata Steel (The Netherlands) and obtained as 0–5.6 mm size grains after the pretreatments of crushing and sieving. Before the experiment, it was milled externally. Fig. 1 shows the particle size distribution of BOF slag powder after milling, measured by laser diffraction spectroscopy (Mastersizer 2000, Malvern). The d_{50} is 10.4 μm, and the specific surface area is 333 m^2/kg. The density of the BOF slag is 3.67 g/cm^3, tested by a Helium pycnometer (AccuPyc™ II 1340). The quantitative chemical and mineralogical compositions are presented in Table 1, characterized by the XRF (Epsilon 3, Malvern PANalytical) and the XRD (D4 Endeavor, Bruker), respectively.

The activator, Na_4EDTA ($C_{10}H_{12}N_2O_8Na_4$), is a highly soluble white solid. Its solubility is 500 g/L water (at 20 °C), much higher than Na_2EDTA ($C_{10}H_{14}N_2O_8Na_2$) and EDTA ($C_{10}H_{16}N_2O_8$) (105 g/L and 0.1 g/L at 20 °C, respectively) [52], which is beneficial for the application of

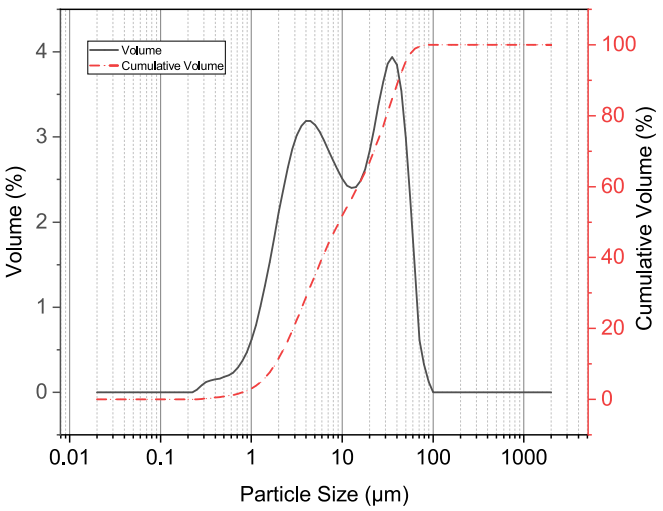

Fig. 1. Particle size distribution of BOF slag.

Table 1
Chemical and mineralogical compositions of raw BOF slag.

Chemical compositions	Content (at.%)	Minerals	Content (wt%)
CaO	40.54	Wuestite	21.9
Fe_2O_3	26.52	Magnetite	4.5
SiO_2	14.50	Brownmillerite	13.0
MgO	7.56	C_2S ($\alpha' + \beta$)	35.4
MnO	4.52	Lime	0.7
Al_2O_3	1.77	Portlandite	0.6
TiO_2	1.64	Calcite	0.3
V_2O_5	0.93	Amorphous	23.6
P_2O_5	1.61		
Cr_2O_3	0.30		
Na_2O	0.11		
GOI[a] 1000	1.4		

[a] Mass gain of ignition (GOI) after BOF slag is heated up to 1000 °C, most likely due to the oxidation of divalent metal ions such as divalent iron.

activator. Additionally, the pH of a 1 wt% solution of Na_4EDTA (11.3) is much higher than that of Na_2EDTA (5.0–5.5), which is more favorable for forming and stabilizing hydration products in a Portland cement-similar system [52]. Na_4EDTA has the highest chelation power within the EDTA compound series because its four carboxyl groups are deprotonated [49]. It is also an intermediate in the commercial synthesis of EDTA, making it highly available [52]. Thus, it was selected from the EDTA compound series to act as the activator in the research. Its

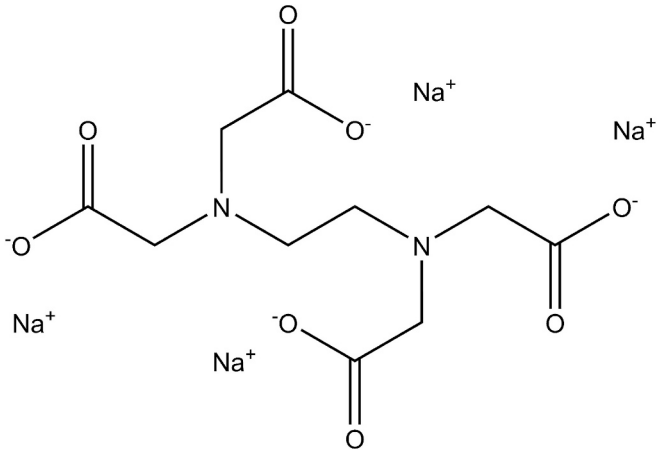

Fig. 2. Chemical structure of Na_4EDTA.

chemical structure is presented in Fig. 2. The technical grade (purity >98 %) monohydrate form of Na_4EDTA ($C_{10}H_{12}N_2Na_4O_8{\cdot}H_2O$) was purchased from Thermo Scientific and used in the research.

2.2. Sample preparation

BOF slag pastes activated by different concentrations of Na_4EDTA were made and cured until the designed dates, as presented in Table 2. The 1.2 wt% Na_4EDTA is equivalent to 1.0 wt% K_3-Citrate (a ligand activator proposed in [8]) in molar terms, which was determined for related discussions in Section 3.5. The sample without Na_4EDTA addition (E00, containing only water) was set as the reference group. Its higher w/b ratio, 0.24, was chosen based on the preliminary test results to achieve adequate and similar workability as Na_4EDTA-activated specimens. First, the Na_4EDTA was added to deionized water, stirred, and then cooled to ambient temperature. After that, the Na_4EDTA solution was mixed with the BOF slag powder in a stainless steel mixer in accordance with EN 196-1 [53]. The paste was stirred for 1 min at low speed and then 2 min at high speed to ensure uniformity. Subsequently, the mixture was cast into a 40 mm × 40 mm × 160 mm prism mold and vibrated 30 times in the jolting apparatus, conforming to EN 196-1 [53]. Then, it was covered with plastic film and stored in a curing box where open bottles containing 1 M NaOH solutions were located to minimize carbonation. The box was placed in a standard curing room (20 °C ± 1 °C and 95 % RH) [53]. After 1 d of casting, all samples were demoulded from the prism mold, and the samples for 7 d and 28 d analysis were sealed with plastic film again and put back into the curing box and room until the designed dates. The demoulded 1 d sample was crushed into small pieces (<1 mm) and immersed in isopropanol for 2 days first and then flushed by diethyl ether in a vacuum filtering pump and then put in the vacuum drying oven at 40 °C for 12 h for hydration stoppage and further characterization analysis. When 7 d and 28 d were reached, the plastic film was removed, and the compressive strength of the samples was tested according to EN 196-1 [53]. The same hydration stoppage procedure was conducted on the crushed fractions after the mechanical test for further characterization.

2.3. Investigation methods

2.3.1. Isothermal calorimetry

The hydration heat of all samples was tracked and recorded by an isothermal conduction microcalorimeter (TAM Air, Thermometric) at a constant 20 °C to investigate the effects of Na_4EDTA on early-age hydration kinetics of BOF slag. The Na_4EDTA concentrations and water/binder (BOF slag) mass ratio are given in Table 2. The BOF slag powder was put into the ampoule first, and then the pre-mixed Na_4EDTA solution was injected inside by the syringe. The mixture was homogenized into a paste by an automatic shaker (TopMix FB15024, Fisher Scientific) and put into the calorimeter immediately. The heat flow baseline was collected in advance to ensure stable conditions. The heat evolution was recorded for 7 days. It needs to be noted that the heat flow data was only integrated after 45 min of inserting the sample to calculate the accumulative heat release accurately. Both heat flow and accumulative heat release were normalized according to the mass of BOF slag powder.

Table 2
Mix design of BOF slag pastes with different Na_4EDTA concentrations.

Samples	Water/binder ratio	Na_4EDTA (wt% of BOF slag)	Curing time (d)
E00	0.24	0.0	1
			7
			28
E12	0.18	1.2	1
			7
			28
E24	0.18	2.4	1
			7
			28
E48	0.18	4.8	1
			7
			28

2.3.2. XRD

The XRD measurement and the quantitative Rietveld refinement were executed to understand the evolution of mineral composition during BOF slag binder hydration with the addition of Na_4EDTA. After the hydration stoppage described in Section 2.2, the BOF slag paste was milled (240 r/m, 10 min) by a planetary ball mill (Pulverisette 5, Fritsch) into powders. The powder was further co-ground with Si powder (325 mesh, Merck Life Science NV, as the internal standard) by an XRD mill (McCrone, RETSCH) for the quantitative analysis [54]. The amount of the Si powder was 10 % of the unspiked sample. The raw BOF slag powder also underwent the same co-grinding procedure with Si for characterization. The XRD pattern was obtained by an X-ray Diffractometer (D4 ENDEAVOR, Bruker) equipped with a LynxEye detector and Co X-ray tube. The experiment was conducted at a stage rotation speed of 30 rpm with a 2θ step size of 0.014° per 1.5 s within the 2θ range of 5–100°. XRD phase identification and quantitative composition determination were conducted by DIFFRAC.EVA software (Bruker) and TOPAS software (Bruker), respectively.

The total mass of solids (after hydration stoppage) changes at different ages of BOF slag hydration since the water is (chemically) bound into hydration products [55]. For a common basis of comparison, the Rietveld refinement results of hydrated samples were corrected (rescaled) into the anhydrous state based on the equation below:

$$W_{rescaled} = W_{Rietveld}\,(1 - H_2O_{bound}) \quad (1)$$

The amount of H_2O_{bound} was calculated from the mass loss (%) below 500 °C in TG analysis (Fig. 7).

The overall hydration degree at each age was calculated by comparing the sum of residual anhydrous phases (wuestite, brownmillerite, C_2S ($\alpha' + \beta$), and lime) with the sum of initial anhydrous phases [55], as shown in equation:

$$\text{Hydration degree} = \left(1 - \frac{\sum W_{rescaled,anhydrous}}{\sum W_{raw,anhydrous}}\right) \times 100\% \quad (2)$$

Phase contents are based on the (rescaled) QXRD results.

2.3.3. TG

The TG/DTG analysis was conducted on the powdered specimen, the same as the XRD analysis (without co-grinding with Si). It was put into the corundum crucible and heated in the TG machine (STA 449 F1 Jupiter, NETZSCH) from 50 °C to 1000 °C at 10 °C/min with the N_2 as the protective atmosphere.

2.3.4. FTIR

The FTIR spectra of hydrated samples at 1 and 28 d were obtained by the Mid-IR scanning (MIR/FIR Spectrometer, PerkinElmer Frontier) based on the attenuated total reflection method (GladiATR). The hydration-stopped and powdered specimens were scanned 20 times between the range of 4000 to 400 cm^{-1} at the resolution of 1 cm^{-1}.

2.3.5. Compressive strength test

The compressive strength of all BOF slag pastes was tested at 7 and 28 d by the strength-testing bench (Controls Automax 5, model 65-L1152/LC) complying with EN 196-1 [56]. Six duplicates were tested for each mix. The average compressive strength and the standard deviation for each mix were recorded.

2.3.6. MIP

Similar to the compressive strength test, Mercury Intrusion Porosimetry (MIP) tests were conducted on samples hydrated for 7d and 28d. Only 1–4 mm grains were sieved out for measurement after the

hydration-stoppage and drying process to minimize the size or ink-bottle effect [57,58]. The porosimeter is AutoPore IV 9500 (Micromeritics) with a maximum working pressure of 228 MPa. The Hg-solid contact angle is 130°, and the Hg surface tension is 485 mN/m.

2.3.7. Leaching analysis

The one-stage batch leaching test was implemented on samples after 28 days of hydration according to EN 12457–2 [59]. Firstly, the hydrated paste was crushed and sieved below 4 mm. The sieved fraction was mixed with deionized water (0.055 μS/cm) at a liquid-to-solid ratio of 10 L/kg. The mixture was agitated by a shaker (ES SM-30, Edmund Buhler) at 300 r/m for 24 h. After shaking and 15 min of settling the suspension, the supernatant was filtered by a 0.2 μm syringe filter (Puradisc™ 25) and acidified by concentrated HNO_3. Finally, the filtrates were analyzed by an inductively coupled plasma atomic emission spectrometer (ICP-AES, SPECTROBLUE) to determine element concentrations.

3. Results and discussion

3.1. Phase assemblage evolution

The XRD patterns of raw BOF slag and hydrated specimens at different ages are shown in Fig. 3, where the main peaks of the major mineral phases were labeled. The quantitative mineral compositions of all samples (excluding Si) determined by Rietveld refinement, as well as the two numerical criteria of fitting, Rwp (residual weighted profile) and GOF (goodness of fit), are shown in Appendix A. Generally, the Rietveld refinement provides a satisfying fitting for XRD patterns of all samples, with GOF range between 1 and 2 and Rwp far below 10 % [55,60]. The rescaled (normalized by raw anhydrous BOF slag, as described in Section 2.3.2) mineral compositions are illustrated in Table 3. Typically, the raw BOF slag is highly crystalline after cooling and solidification [10,61]. However, as seen in Appendix A, there is a significant amount of amorphous phase within raw BOF slag, which could be due to the (partial) amorphization of crystalline phases after disk milling and further XRD milling [62]. It is most likely that the primary source of these amorphized crystalline phases is C_2S, as indicated by a comparison between the large-area phase mapping analysis based on the PhAse Recognition and Characterization (PARC) software and XRD Rietveld refinement [8,10]. The PARC software was previously described in detail [63].

As can be seen from Fig. 3 and Table 3, the main crystalline hydration products of BOF slag (with or without Na_4EDTA activation) are the hydrogarnet, accompanied by a small amount of hydrotalcite. The introduction of Na_4EDTA does not alter the species of hydration products. Hydrogarnets are a series of minerals with the common general chemical formula $Ca_3(Al_xFe_{1-x})_2(SiO_4)_y(OH)_{4(3-y)}$ that consist of linked polyhedral [8] [66]. It is observed in hydrated OPC systems or calcium aluminate blended cement incorporating iron-rich slag [28,64]. Due to the (partial or complete) inter-substitution of Al^{3+} and Fe^{3+}, SiO_4^{4-} and $4OH^-$, it is hard to determine the definite chemical formula of hydrogarnet, and the peaks of hydrogarnet in the XRD pattern tend to be broad [8,10]. Besides, within silica-free hydrogarnets, the C_3FH_6 (Fe-katoite) is an unstable phase [29]. Thus, to quantify hydrogarnet accurately within hydrated BOF slag, two crystal structures (end-members), katoite ($Ca_3Al_2(OH)_{12}$, ICSD# 202315) and hydroandradite ($Ca_3Fe_2(SiO_4)_{1.15}(OH)_{7.4}$, ICSD# 29247) were applied in the Rietveld refinement process without inclusion of the C_3FH_6 (Fe-katoite). Likewise, the situation also applies to another crystalline hydration product, the hydrotalcite (series), which is a kind of (distorted) brucite-like layered double hydroxides (LDHs) with the general formula $Mg_6Al_{2-x}Fe_x(CO_3)_y(OH)_{(18-2y)}\cdot nH_2O$ that consists of $[(M^{2+}_{1-x}M^{3+}_x)(OH)_2]^{x+}$ main layers and intercalated anions. Due to the possible substitution of Mg^{2+} by trivalent cations (Al^{3+} and Fe^{3+}) within double-hydroxide main layers, CO_3^{2-}, OH^- (also other possible anions) and water molecules are incorporated in the interlayer region to compensate for the net positive charge in this case [65]. It is also hard to determine the actual substitution ratio of Mg^{2+} by Al^{3+} and Fe^{3+}, as well as the anion species and ratios. Hence, two end members hydrotalcite ($Mg_{0.667}Al_{0.333}(OH)_2(CO_3)_{0.167}(H_2O)_{0.5}$, ICSD# 81963) and pyroaurite ($Mg_6Fe_2(OH)_{16}(CO_3)(H_2O)_{4.5}$, ICSD# 80876) were used in the Rietveld refinement [65]. Hereinafter, hydrogarnet and hydrotalcite refer to the hydrogarnet and hydrotalcite mineral series for discussion. Also, C_2S stands for C_2S ($\alpha' + \beta$).

According to Table 3, C_2S decreases significantly from 35.4 wt% in raw BOF slag to 24.6 wt% in sample E48 after 1 day of hydration. In contrast, in samples with low doses or without Na_4EDTA application, less or almost no C_2S has reacted. As described in the introduction, this should be mainly attributed to its intrinsic low early hydration reactivity and the embedded impurities. Introducing Na_4EDTA (especially high dose) significantly promotes the early depletion of C_2S. The corresponding hydration product should be mainly the amorphous C-S-H

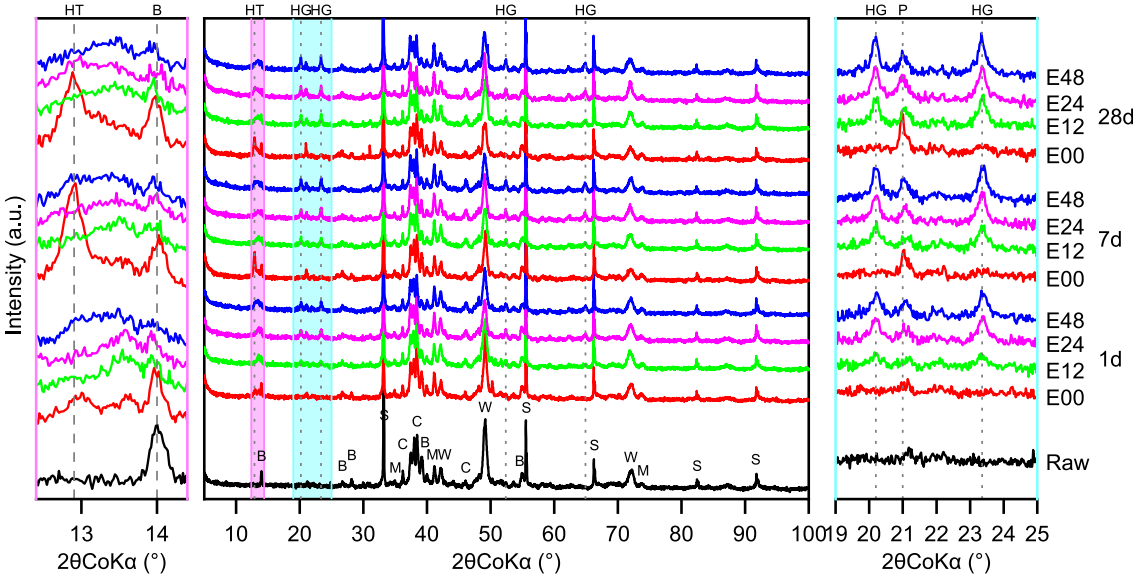

Fig. 3. XRD patterns (global and locally zoomed-in views) of raw BOF slag and hydrated samples (Legends mean: B-Brownmillerite, C-C_2S (belite), M-Magnetite, W-Wuestite, HT-hydrotalcite (series), HG-Hydrogarnet (series), P-Portlandite, S-Si).

Table 3
Quantitative mineralogical compositions of raw and corrected (rescaled) hydrated BOF slag (g/100 g of raw anhydrous BOF slag). [Anhydrous] represents the sum of four (rescaled) (residual) anhydrous phases: wuestite, brownmillerite, C_2S ($\alpha' + \beta$), and lime.

Phase	Raw BOF	1 d				7 d				28 d			
		E00	E12	E24	E48	E00	E12	E24	E48	E00	E12	E24	E48
Wuestite	21.9	20.8	18.4	15.3	14.3	19.8	14.1	13.9	13.1	18.2	15.6	14.0	14.4
Magnetite	4.9	4.9	4.1	4.3	3.7	4.8	4.1	3.6	3.7	4.7	3.9	3.6	3.6
Brownmillerite	13.0	11.6	6.6	5.4	3.6	10.5	5.4	5.3	4.0	10.5	4.9	3.7	3.5
C_2S ($\alpha' + \beta$)	35.4	33.9	30.5	27.8	24.6	30.4	27.3	24.9	24.4	27.9	24.7	23.8	21.0
Hydrogarnet	0.0	1.6	5.0	8.9	8.6	2.3	7.9	9.2	11.2	2.8	8.6	11.4	11.6
Hydrotalcite	0.0	1.9	2.8	4.1	3.7	3.1	2.9	2.2	2.7	3.3	2.5	3.1	3.4
Lime	0.7	0.1	0.3	0.2	0.4	0.1	0.1	0.6	0.3	0.2	0.3	0.3	0.1
Portlandite	0.2	0.1	0.1	0.2	0.4	0.7	0.1	0.3	0.6	1.1	0.4	0.9	0.7
Calcite	0.3	0.3	0.5	0.9	0.6	0.5	0.6	0.8	0.8	0.8	0.9	0.8	1.0
Amorphous	23.6	21.9	27.6	26.2	33.9	22.6	31.9	33.3	31.6	24.3	31.8	32.0	32.5
[Anhydrous]	71.0	66.3	55.9	48.7	42.9	60.9	46.9	44.6	41.8	56.8	45.5	41.8	39.0

phase and a minor portlandite [5,10,16,67]. This inference could be verified by the higher amorphous content within E48 while also containing a similar amount of crystalline hydration products (hydrogarnet and hydrotalcite) as E24. From 1 to 7 d, C_2S within E12 and E24 is consumed further, while the amount in E48 remains stable. The C_2S in the control specimen E00 also decreases from 33.9 to 30.4 wt%. At 28 d, the situation is similar to 1 d: the C_2S content is lower in samples with a higher Na_4EDTA dosage. It also needs to be noted that, as discussed above, part of the C_2S may exist as amorphous content in the unreacted slag. It is, therefore, difficult to tell how much of the amorphous content in the hydrated samples is due to newly generated hydration products and how much of the original amorphous C_2S is still present. Even so, according to Fig. 3 and Table 3, Na_4EDTA has distinct effects on the formation of hydrogarnet and hydrotalcite. Na_4EDTA promotes the formation of hydrogarnet at each age, while at later ages (7 and 28 d), Na_4EDTA inhibits the formation of hydrotalcite instead. Considering the different compositions of hydrogarnet ($Ca_3(Al_xFe_{1-x})_2(SiO_4)_y(OH)_{4(3-y)}$) (Si-bearing) and hydrotalcite ($Mg_6Al_{2-x}Fe_x(CO_3)_y(OH)_{(18-2y)}\cdot nH_2O$) (Si-free), this indirectly suggests that Na_4EDTA significantly promotes the dissolution of C_2S in BOF slag, thereby promoting the formation of C-S-H and hydrogarnet.

Brownmillerite presents a different trend from C_2S. Within all Na_4EDTA-activated samples, its hydration is almost entirely completed after 1 d. For example, the brownmillerite decreases from 13.0 wt% to 3.6 wt% in E48. This effect is enhanced as the Na_4EDTA content increases. At later ages, the brownmillerite depletes further slightly in E12 and E24 and stays almost constant within E48. In comparison, in E00, the brownmillerite shows little reduction during the whole hydration period due to its low reactivity. Obviously, Na_4EDTA has a significant promoting effect on brownmillerite hydration (depletion), and most of the reaction occurs within one day. This effect is enhanced as the Na_4EDTA content increases, although brownmillerite hydration is already prominently enhanced at just 1.2 wt% Na_4EDTA. In contrast, C_2S dissolves significantly only at the highest dose of Na_4EDTA. Since the hydration capacity of brownmillerite itself is deficient, it can be inferred that, in the BOF slag system, $EDTA^{4-}$ tends to preferentially promote the dissolution of brownmillerite before C_2S. This phenomenon can be attributed to the decreasing chelation (complexation) affinity of $EDTA^{4-}$ for metals from iron to calcium [48,68,69], which is discussed in more detail in Section 3.5.

Another iron-based mineral, wuestite, presented a similar trend as brownmillerite, though with a much lower hydration degree. In E24 and E48, most of the wuestite dissolution finishes within the first day, and after that, little further reaction is observed. In contrast, the content of wuestite does not decrease noticeably within E12 until 7 d. It seems that a high dose of Na_4EDTA also improves the dissolution and total hydration extent of wustite. The wuestite content in E00 also shows a minor decrease with the increase of hydration age, which could be attributed to the reaction of Mg [70,71]. As the hydration continues, pH increases, which favors the dissolution of the wuestite that hosts Mg [72,73]. After just 1 day of hydration, within E24 and E48, the majority of the crystalline hydration products have formed. Between 1 and 28 d, their content remains relatively stable or only slightly increases. Their formation trend is generally consistent with the hydration (consumption) of brownmillerite and wuestite which are the source of the Fe and, to a much lesser extent, Al in the hydration products.

In all hydrated samples, little portlandite is generated. However, at 7 and 28 d, in the reference sample E00, portlandite shows a slightly stronger peak than in Na_4EDTA-activated samples. As discussed above, the hydration of C_2S is significantly enhanced within high-dose-Na_4EDTA-activated samples, and the corresponding amorphous product (C-S-H gel) increases accordingly. The lower portlandite formation within Na_4EDTA-activated specimens could be attributed to the (partial) capture of calcium ions by $EDTA^{4-}$ and related possible inhibition of portlandite nucleation and growth [74].

Fig. 4 gives the overall hydration degree of all samples at three ages based on Eq. (2) and the sum of four residual anhydrous phases expressed as [anhydrous] in Table 3. It is clear that Na_4EDTA significantly promotes the hydration of the whole BOF slag, especially at early ages, and the enhancement effect increases with the increase of Na_4EDTA dosage. For example, after only 1 d, 39.6 % of the E48 sample hydrates, while the hydration degree of the control sample E00 is only 6.6 %. With age increase, E48 does not show a significant increase in hydration degree, while the samples with lower Na_4EDTA doses show a

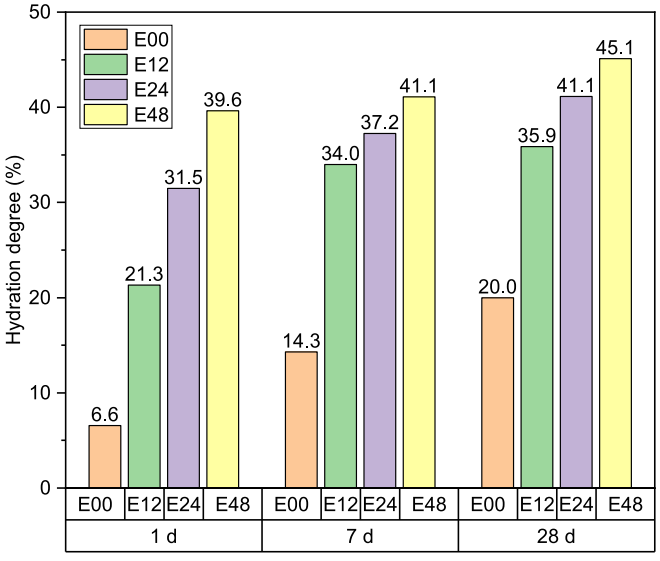

Fig. 4. Hydration degree calculated based on the sum of four residual anhydrous phases.

more obvious increase.

TG/DTG analysis was conducted to supplement the QXRD analysis. Fig. 5 shows TG/DTG curves of Na_4EDTA-activated BOF slag pastes compared with the control sample E00 at 1, 7, and 28 d. All Na_4EDTA-activated specimens present higher total mass loss than the control sample E00 at any age, and the mass loss increases with the doses of Na_4EDTA. For example, after 1 day of hydration, it increases from 3.1 wt % in E12 to 9.1 wt% in E48.

The mass loss below 200 °C could be most likely attributed to the dehydration of the C-S-H phase [55,75]. After 1 day of hydration, Na_4EDTA evidently enhances the formation of the C-S-H phase, though this promotion effect does not demonstrate a strict linear correlation with increasing Na_4EDTA dosage. As hydration progresses, this promoting effect becomes less pronounced while still discernible, which is consistent with the QXRD analysis.

The mass loss between 200 °C to 400 °C can be attributed to the water loss of hydrogarnet and hydrotalcite [29,76], including the gradual loss of interlayer water (for hydrotalcite) and hydroxyl groups dehydroxylation (for both phases). Across all hydration ages, the introduction of Na_4EDTA promotes the formation of these two main crystalline hydration products, and the amount increases with the increase of Na_4EDTA dosage. For instance, the mass loss ranges from 1.1 wt% in the reference sample E00 to 2.6 wt% in E48 at 1 d. The enhanced formation of hydrogarnet and hydrotalcite in Na_4EDTA-activated samples primarily takes place within the first day. Beyond this initial period, minimal changes are observed, while the hydration continues at later ages. The overall trend is generally in agreement with the XRD analysis. The peak at around 465 °C could be easily attributed to the decomposition of portlandite [30,77]. It is more apparent at later hydration ages (7 and 28 d) in the reference sample E00, which also correlates well with the XRD analysis.

The mass loss between 600 and 800 °C is typically for the decarbonation of calcium carbonate, as clearly shown by the 1d E00 DTG curve in Fig. 5a [78,79]. However, in addition to the decarbonation of calcium carbonate, within 500 to 800 °C, a more significant mass loss can be observed for the Na_4EDTA-activated samples, and this mass loss generally increases with the Na_4EDTA dosage at each age. According to the QXRD analysis, introducing Na_4EDTA does not cause a significant difference in the calcium carbonate content between corresponding Na_4EDTA-activated samples and the reference specimen. It can be inferred that the enhanced mass loss here is possibly caused by the decarbonation of carbonate anions from the interlayer of hydrotalcite [65,80]. However, at later ages, the reference sample E00 has a slightly higher amount of hydrotalcite than most Na_4EDTA-activated specimens, as shown in Table 3. Hence, it is reasonable to infer that the EDTA complexes themselves contribute to the mass loss within this temperature range due to their decomposition [81]. The difference in mass loss within 500 to 800 °C between the reference sample and Na_4EDTA-activated specimens is getting larger with age. For example, the difference between E00 and E48 increases from 2.2 wt% at 1 d to 2.9 wt% at 28 d. It indicates that, as the hydration proceeds, the EDTA complexes are more incorporated into the hydration products. Otherwise, unbound EDTA complexes are removed when the hydration of the sample is stopped.

The FTIR-ATR test was performed to verify this conjecture, and the spectra are presented in Fig. 6. The infrared peaks at 1587 cm^{-1} in Na_4EDTA-activated pastes can be attributed to the asymmetric stretching vibration of the COO^- group, which indicates the presence of EDTA (complexes) within the hydration products [82–84]. As shown in Fig. 6a, at 1 d, the $V_{as}(COO^-)$ peak could be easily observed, but it does not show a pronounced difference among the samples activated by different Na_4EDTA concentrations. This situation indicates a weak retention of EDTA (complexes), which is as expected and could be attributed to the high solubility of $[M\text{-}EDTA]^{n-}$ complexes [50]. At 28 d, samples from E12, E24, and E48 show increasingly stronger $V_{as}(COO^-)$ absorption peaks, which reveals prominently enhanced incorporation degree of

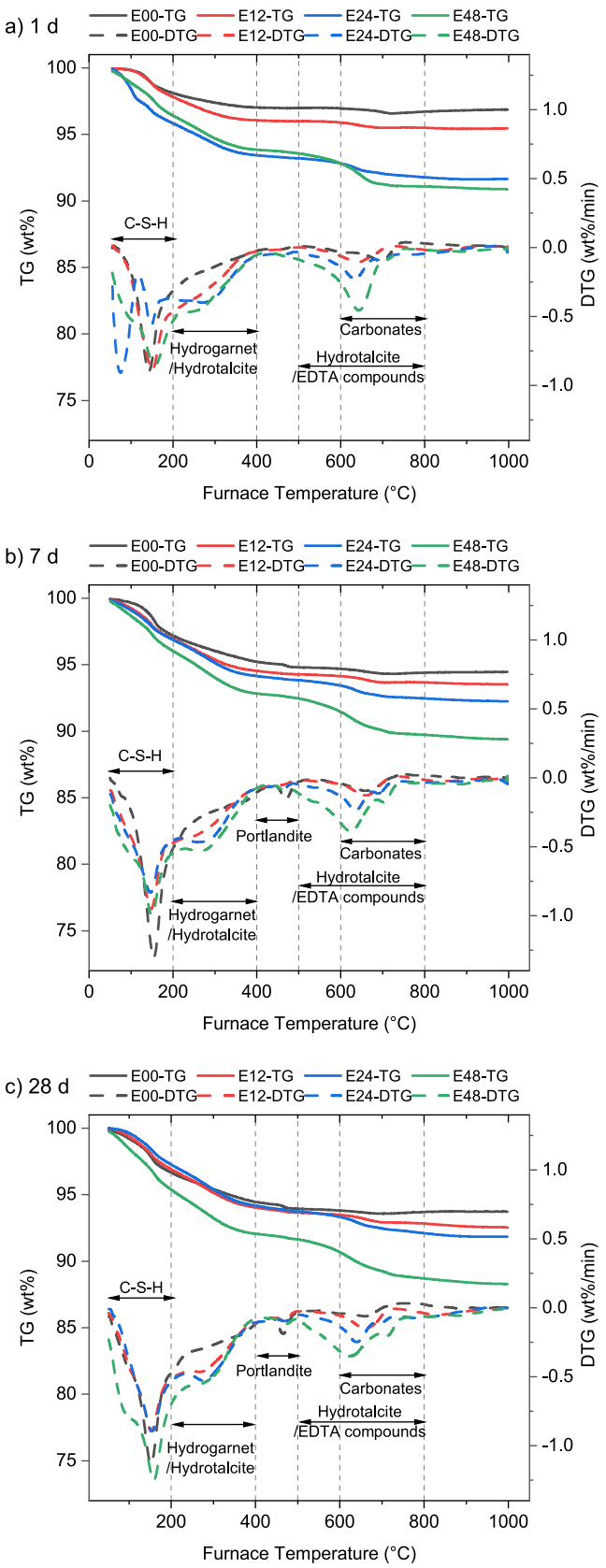

Fig. 5. TG/DTG curves of hydrated BOF slag paste at 1, 7, and 28 d.

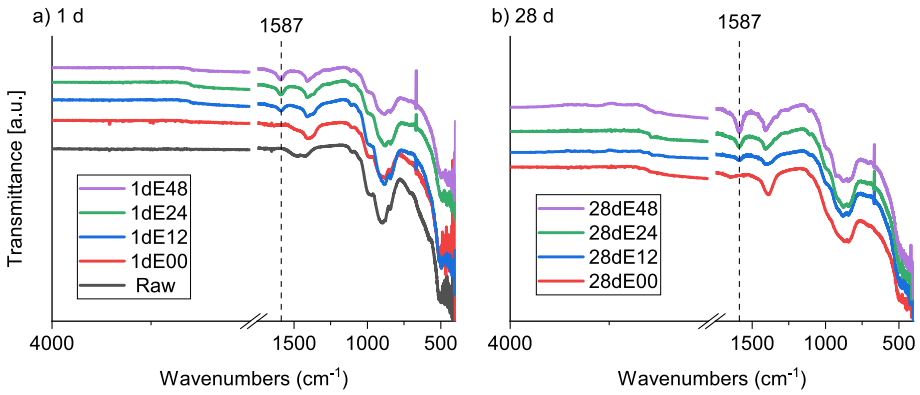

Fig. 6. FTIR spectra of hydrated BOF slag pastes and raw BOF slag.

EDTA (complexes) into the hydration product. The interlayer region of the hydrotalcite is possibly the leading retention location of EDTA (complexes) [85], as analyzed in Section 3.5 and shown in Appendix C. Based on the above analysis, the mass loss between 500 and 800 °C is categorized as hydrotalcite/EDTA compounds.

Typically, in cementitious systems, mass loss below 600 °C is categorized as the loss of water [55]. Here, as discussed above, the mass loss of 500–600 °C is possibly related to the decarbonates or decarboxylates of hydrotalcite and EDTA compounds in this specific system. The mass loss below 500 °C (H_2O_{bound} as described in Section 2.3.2) of all hydrated specimens at different ages was calculated and presented in Fig. 7. This generally indicates enhanced hydration in Na_4EDTA-activated samples at all stages, and it is particularly strong at early ages (particularly at 1 d).

3.2. Early hydration kinetics

Fig. 8 demonstrates the heat flow and cumulative heat release curves (normalized by mass of BOF slag) of all specimens during the first 72 h and 7 d, respectively. As shown in Fig. 8a, the control sample E00 shows no noticeable exothermic peak at early ages. In the first 5 h, the heat flow curves of Na_4EDTA-activated samples basically overlap and are much higher than that of the reference sample E00, which indicates a much more prominent dissolution of reactive phases within Na_4EDTA-activated specimens. The introduction of Na_4EDTA also induces pronounced hydration peaks after initial dissolution heat release. There are no apparent induction periods before the main hydration heat peaks, as discussed in detail later. It can be inferred that $EDTA^{4-}$ acts as an activator and accelerator in the BOF slag system, even in early hydration. The trend is distinct from the findings in other cementitious systems, such as OPC, calcium sulphoaluminate belite cement (CSBC), and magnesium oxysulfate (MOS) cement, where EDTA (or its salt derivatives) retards the early age hydration [46–48], which should be attributed to the enormous difference in chemical composition between them and BOF slag, with BOF slag containing much more iron and elevated levels of unfavorable elements such as Mn, Ti, and V. For example, OPC typically contains only ~2–3 wt% Fe_2O_3 (e.g., 2.9 or 2.75 wt% in CEM I 42.5 Portland cement) [86,87], whereas BOF slag contains 20–40 wt% Fe_2O_3. In OPC, the major matrix-constituting elements, Ca, Si, and Al, have good solubilities themselves. Hence, the chelation with $EDTA^{4-}$ actually increases the amount of time needed to achieve supersaturation of the aqueous environment, thus hindering the nucleation and growth of relevant hydration products [88,89]. By contrast, BOF slag is much less reactive, and $EDTA^{4-}$ tends to preferentially chelate with Fe and other unfavorable elements (e.g., Mn, Ti, and V) rather than Ca due to $EDTA^{4-}$ higher chelation affinities toward Fe and these elements [50,68,90], as discussed in Section 3.5. This preferential chelation (sequestration) enhances the dissolution of silicate and ferrite phases, accelerates the release of SiO_4^{4-}, and promotes the rapid formation of hydrogarnet and C–S–H.

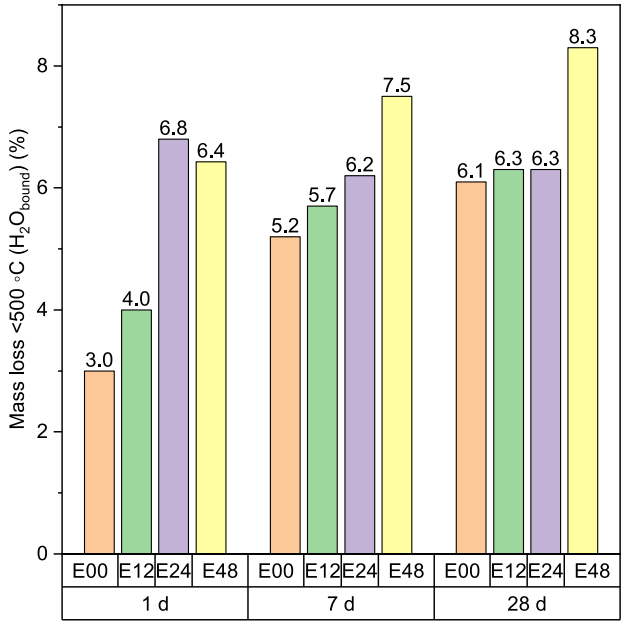

Fig. 7. Mass loss below 500 °C (H_2O_{bound}) of hydrated samples after TG/DTG analysis.

For E12, the two prominent heat release peaks appear at 6.5 h and 11 h, which could be mainly attributed to the hydration of brownmillerite and relevant product formation based on the intrinsic hydration rate discussion in the introduction and the 1 d QXRD analysis. The increase of Na_4EDTA dosage retards these two peaks in E24 and E48 and reduces the peak height, indicating a relatively similar retardation effect as observed in other cementitious systems, which may be due to the partial chemical blocking of frame-forming metal ions by excessive $EDTA^{4-}$, as analyzed in Section 3.5. Another relatively pronounced exothermic peak appears in E48 at around 24 h (slightly later and apparently lower in E24), which, combined with the 1 d QXRD analysis, can be primarily attributed to the hydration of C_2S. Na_4EDTA-activated samples also present a much higher cumulative heat release than the reference E00 after 7 days of hydration, as shown in Fig. 8b. These indicate the apparent promotion effects of Na_4EDTA on BOF slag early hydration and are consistent with the QXRD and TG/DTG analysis. As mentioned before, there is almost no induction stage for the exothermic curves of Na_4EDTA-activated samples. In other words, with Na_4EDTA, the concentration of hydration product-constituting ions (primarily Ca^{2+} and SiO_4^{4-} in this specific system) in the aqueous environment reaches saturation and starts to precipitate quickly. This phenomenon should be attributed to the fast adsorption and extraordinary chelation

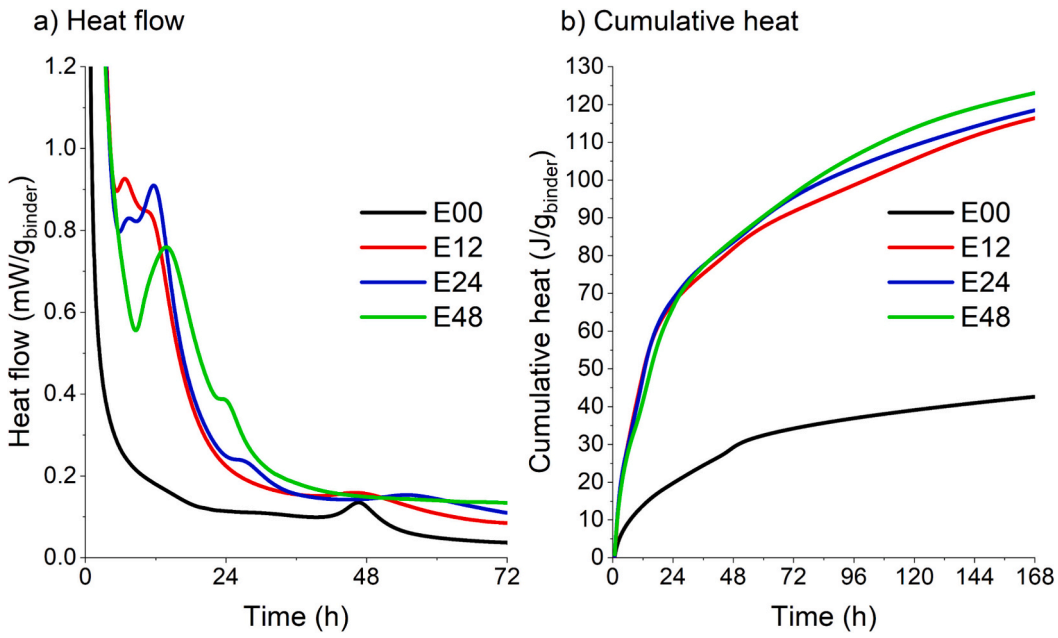

Fig. 8. Heat flow and cumulative heat of BOF slag paste early hydration (with/without Na_4EDTA).

capacity of $EDTA^{4-}$ and its higher affinity to Fe and other unfavorable elements (such as Mn, Ti, V) compared to Ca [50,68,90]. As discussed above, while Na_4EDTA chelates Fe and other unfavorable elements, it promotes the dissolution of hydraulically reactive phases (brownmillerite and silicates) and increases the Ca and Si concentration in the solution, which leads to quicker saturation and promotes hydrogarnet and C–S–H precipitation. The distinct affinities of $EDTA^{4-}$ to different metals will be discussed in Section 3.5.

3.3. Microstructural and mechanical properties

For cementitious materials, porosimetry is a vital property affecting both mechanical performance and durability. Based on the MIP test, the total porosity and pore size distribution of all BOF slag pastes at 7 and 28 d are shown in Fig. 9. As shown in Fig. 9a, Na_4EDTA-activated specimens illustrate lower total porosities than the reference sample E00 at each age. Besides, at 28 d, E48 shows a much lower total porosity, 14.9 %, compared with the reference or specimens activated by lower concentrations of Na_4EDTA. Based on the pore size, pores are categorized as gel pore (<10 nm), middle capillary pore (10–50 nm), capillary pore (50–100 nm), and macro pore (>100 nm) here [91,92]. Fig. 9b presents the pore size distribution according to this classification criteria. In general, it can be seen that using Na_4EDTA reduces the total porosity and refines the pore size distribution of the samples. At 7 d, in Na_4EDTA-activated specimens, compared with the control sample E00, the proportion of macro pores is significantly reduced, and that of the middle

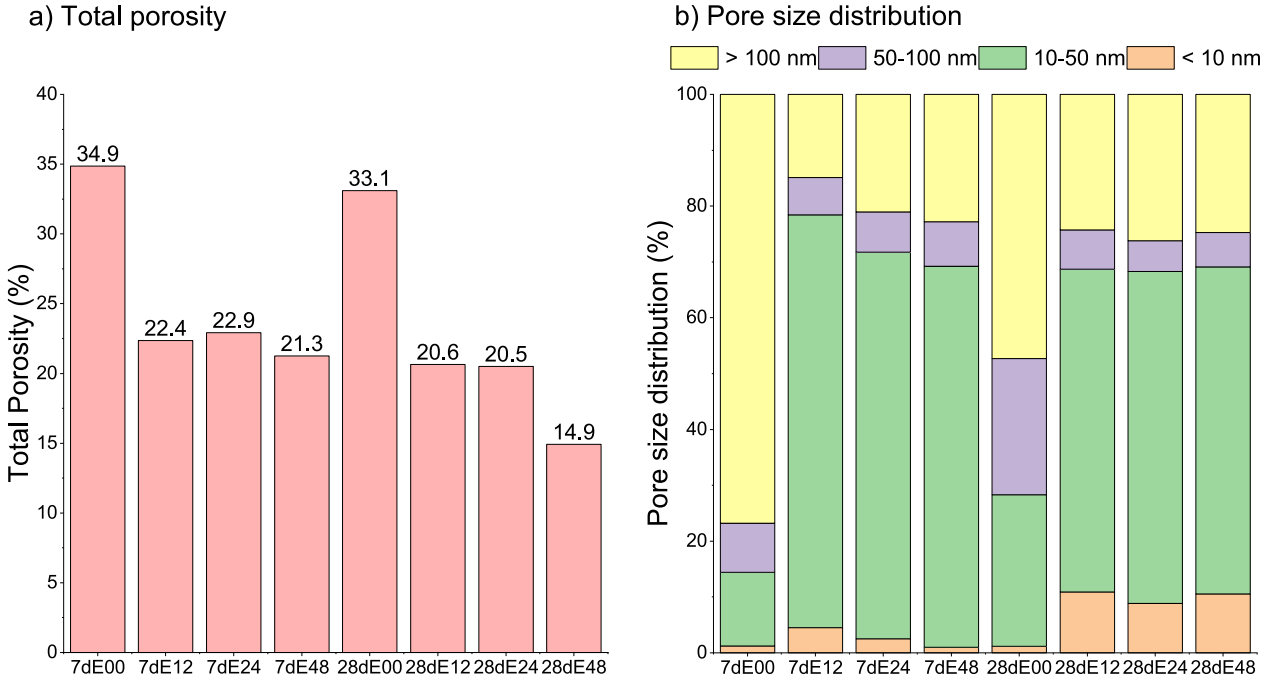

Fig. 9. Total porosity and pore size distribution of all BOF slag paste at 7 and 28 d.

capillary pore increases prominently. There is also a slight increase in the proportion of gel pores. After 28 days of hydration, the pore distribution of the reference sample is also refined, but the ratio of macro pores and capillary pores is still high. In contrast, compared with the E00 sample, the capillary pores proportion of Na_4EDTA-activated samples decreases, with the proportion of middle capillary and gel pores increasing significantly. Overall, according to the MIP test results, it can be concluded that the activation of Na_4EDTA reduces the total porosity and refines the pore size distribution, which agrees well with the phase assemblage characterizations.

The compressive strength of all hydrated samples at 7 and 28 d is presented in Fig. 10 to illustrate the effects of Na_4EDTA on the macroscopic mechanical performance of the stand-alone BOF slag binder. It is clear that without Na_4EDTA activation, the control sample E00 only gains insufficient strength, 2.9 MPa, at 7 d. After 28 days, the value for E00 increases compared with that of 7 d, yet it is still unsatisfactory. In contrast, all Na_4EDTA-activated specimens present an order of magnitude higher compressive strength than the reference sample E00 at 7 d. As discussed in Section 3.1, this phenomenon should be primarily attributed to the markedly enhanced dissolution of silicate and significantly promoted formation of C-S-H and hydrogarnet. Na_4EDTA-activated samples also show an evident compressive strength increase from 7 to 28 d. However, the increase rate is not as significant as that of the reference sample E00, which is to be expected and should be attributed to the prominently enhanced early hydration degree with the usage of Na_4EDTA, which correlates well with the previous analysis. In general, at each age, Na_4EDTA-activated samples show higher compressive strength, with the strength increasing as the Na_4EDTA dosage increases.

3.4. Leaching evaluation

As outlined in the introduction, previous studies have indicated that BOF slag may pose environmental risks due to the presence of potentially toxic elements, primarily V and Cr [2,12,72,93,94]. To assess the effects of Na_4EDTA on leaching possibilities and heavy metal immobilization capacity of BOF slag binder, the one-stage batch leaching test was conducted on all BOF slag pastes after 28 days of hydration. The concentrations of leached contaminant metal ions and the legal limits specified by the Dutch Soil Quality Code (DSQC) are presented in Table 4 [95]. The DSQC defines the environmental requirements that building materials must meet to be used in the Netherlands.

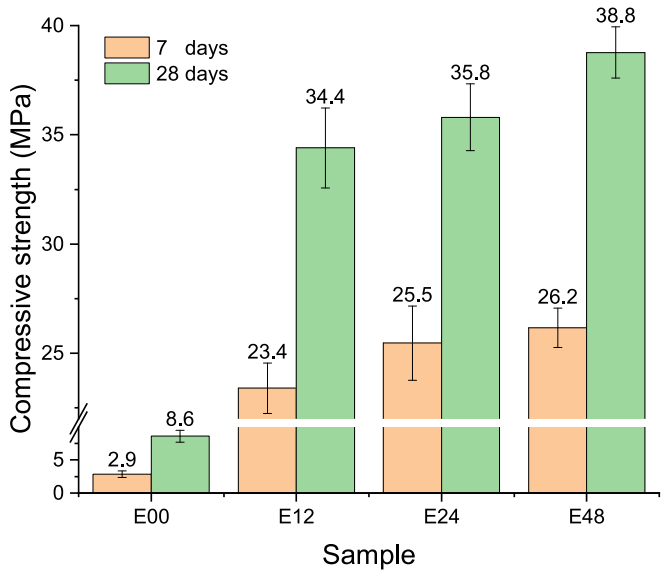

Fig. 10. Compressive strength of BOF slag pastes after 7 and 28 days of hydration.

Table 4
Leaching of potentially toxic metal ions from hydrated BOF slag pastes at 28 d and the legal limits (mg/kg).

Elements	Unshaped material DSQC	Raw BOF slag	E00	E12	E24	E48
Ba	22	UDT[a]	6.310	4.730	5.180	4.930
Cr	0.63	0.24	0.010	0.060	0.080	0.140
Mo	1.0	0.02	0.040	0.060	0.080	0.110
V	1.8	3.66	0.020	0.530	0.490	0.790
Zn	4.5	UDT	0.020	0.020	0.020	0.030
pH	/	12.2	12.7	12.7	12.7	12.8

[a] Under detection threshold: Ag, As, Be, Bi, Cd, Co, Cu, Ga, In, Ni, Hg, Pb, Sb, Se, Sn.

Existing research shows that, within BOF slag, Cr partially exists in a trivalent form, occupying octahedral coordination sites within the brownmillerite ($C_2(A,F)$) phase, while the remaining Cr is mainly incorporated into the RO solid solution (in the wuestite structure) [10,72,93,94]. Typically, minimal Cr is released and remains in its less toxic trivalent state during natural aging or even after leaching [93,94,96]. Vanadium (V) is found in the tetravalent state (mean of trivalent state at octahedral coordination and pentavalent state at tetrahedral coordination), in brownmillerite ($C_2(A,F)$) and belite (C_2S ($\alpha' + \beta$)) [13,72,97–99]. V(III) readily oxidizes to the pentavalent form (its most toxic and mobile state) as coordination symmetry decreases from octahedral to tetrahedral during natural aging or oxidation processes [93,94,99]. Compared to Cr, V generally exhibits more severe leaching. Additionally, V is present in higher concentrations within the original BOF slag than Cr, as shown in Table 1. Thus, V presents a greater potential for environmental harm and warrants careful attention.

As seen from Table 4, as expected, the V leaching of the raw BOF slag exceeds twice the legal limit for unshaped (granular) material. Cr leaching can also be observed but is below the legal limit. Leaching values for all hydrated BOF slag pastes (including the reference sample E00) are below the legal limits, which indicates a satisfying immobilization of these elements in the hydration products. It could be attributed to the uptake in hydrogarnet or hydrotalcite at Al(III) or Fe(III) octahedral coordination (for Cr(III) and V(III)) [100,101] or (partially) replacing the SiO_4^{4-} or $H_4O_4^{4-}$ tetrahedral (VO_4^{3-}) in C-S-H or hydrogarnet [102,103], or embedding in the interlayer region of hydrotalcite (VO_4^{3-}) [101,104–107].

Compared with the reference specimen E00, Na_4EDTA-activated samples demonstrate noticeably higher leaching of Cr and V, particularly V, with this effect intensifying as the Na_4EDTA dosage increases. This phenomenon can be attributed to the extraordinary chelating power of $EDTA^{4-}$ toward almost all transition metals, forming highly soluble (and therefore leachable) [M-EDTA] complex ions, such as Cr-EDTA and V-EDTA here [46–48,50,68,108]. Consequently, although a portion of Cr and V is incorporated into the hydration products, as previously analyzed, a non-negligible fraction likely remains dissolved in the aqueous environment. The introduction of Na_4EDTA exacerbates V leaching more severely than Cr leaching. One potential reason for this disparity is that a considerable portion of Cr is confined within the RO phase, rendering it less susceptible to Na_4EDTA effects throughout the process.

3.5. Metal-EDTA chelation mechanism

The Metal-EDTA chelation mechanism was discussed to provide insights into the enhanced hydration of BOF slag activated by Na_4EDTA. Except for the potentially toxic metal ions presented in Table 4, the amount of dissolved Fe, Mg, and Mn elements in the leachate was also detected, as presented in Fig. 11. They are abundant elements within BOF slag and are generally insoluble. Considering the essentially identical pH, and the huge difference in leached metals between the reference sample E00 and the EDTA-activated samples, it can be inferred that

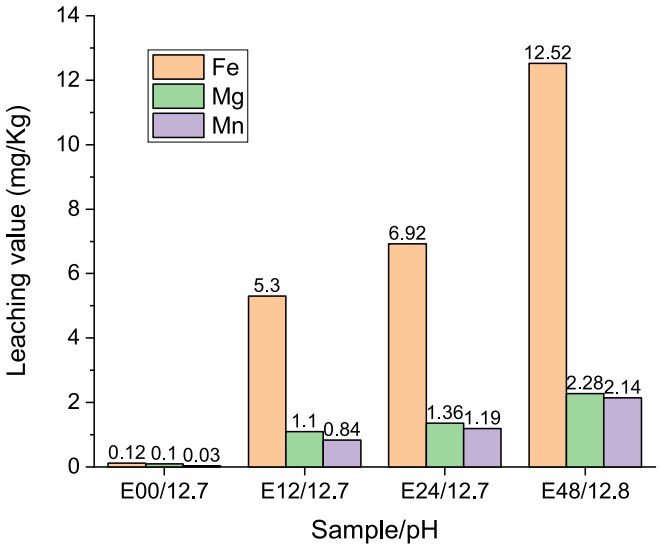

Fig. 11. Leaching values of abundant, non-toxic metal elements from hydrated specimens after 28 d.

soluble $[M\text{-}EDTA]^{n-}$ complexes are the primary leaching forms of these three metals in EDTA-activated samples. Using Na_4EDTA promotes the leaching of these three elements, and the effect increases with the dose.

When metal oxides (minerals) are dissolved in water, the corresponding metal ions, such as Fe, exist as free-moving complexes ($[Fe(H_2O)_6]^{3+}$) coordinated by six polar molecules (H_2O) [41], as shown in Fig. 12a. However, iron oxides are generally highly insoluble in a neutral or alkaline environment. In contrast to this situation, the adsorption of EDTA ($^{4-}$) onto the mineral surface and the strong chelation (complexation) reaction between Fe and EDTA ($^{4-}$) (transferring of lone electron pairs from electron donors "O" and "N" to "Fe") with the formation of stable $[Fe\text{-}EDTA]^-$ complexes (Fig. 12b) can disrupt the crystal lattice of iron oxides, thus promoting iron dissolution [41,50,68].

The chelation (complexation) reaction proceeds as a dynamic equilibrium, as shown by the equation below:

$$EDTA^{4-} + M^{n+} \rightleftharpoons [M-EDTA]^{(n-4)-} \quad (3)$$

Thus, the affinity of $EDTA^{4-}$ to chelate with different metal ions generally depends on the equilibrium constant, namely, the (standard) stability constant of the complex ions [50,81]. It is expressed in the equation:

$$K_S = \frac{([M-EDTA])^{(4-n)-}}{(M^{n+})(EDTA)^{4-}} \quad (4)$$

It thus can be used to predict the chelation preference of $EDTA^{4-}$ for varying metal ions. In a system containing multiple metal ions, $EDTA^{4-}$ will chelate with ions in order of decreasing stability constant (K_S). The standard Log K_S (with 0.1 M KCl as background electrolyte in $T = 20$ °C) for Fe^{3+} and Ca^{2+} are 25.1 and 10.7, respectively [109,110], which indicates that $[Fe\text{-}EDTA]^-$ is much more stable than $[Ca\text{-}EDTA]^{2-}$, meaning that calcium ions will only be complexed when $EDTA^{4-}$ is in excess, beyond the amount required for iron chelation. This principle aligns with findings in this study: the activating effect of Na_4EDTA on brownmillerite is considerably more pronounced than on C_2S, with significant consumption of C_2S occurring only at higher Na_4EDTA concentrations. Furthermore, as shown in Table 4, V leaching increases more than Cr leaching with rising Na_4EDTA doses. Beyond the partial retention of Cr in the (relatively stable) RO phase, the higher (standard) stability constant (Log K_S) of V(III)-EDTA (25.9) compared to Cr(III)-EDTA (23.4) is also a significant factor [111,112].

In addition to a ligand's affinity for specific metal ions (minerals), the varying stability constants of different ligands complexing with the same metal ions can reveal their differing capacities to promote dissolution and hydration. Fig. 13 compares the 7 d hydration degree (based on

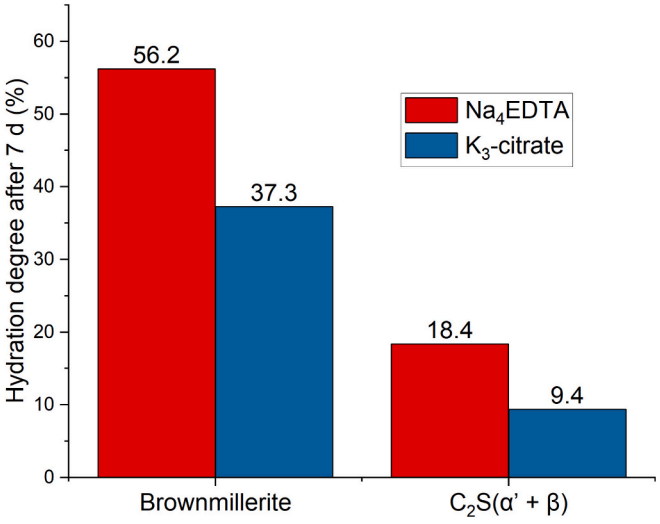

Fig. 13. Early hydration degree (7 d) of BOF slag activated by 1 wt% of K_3-citrate and 1.2 wt% of Na_4EDTA.

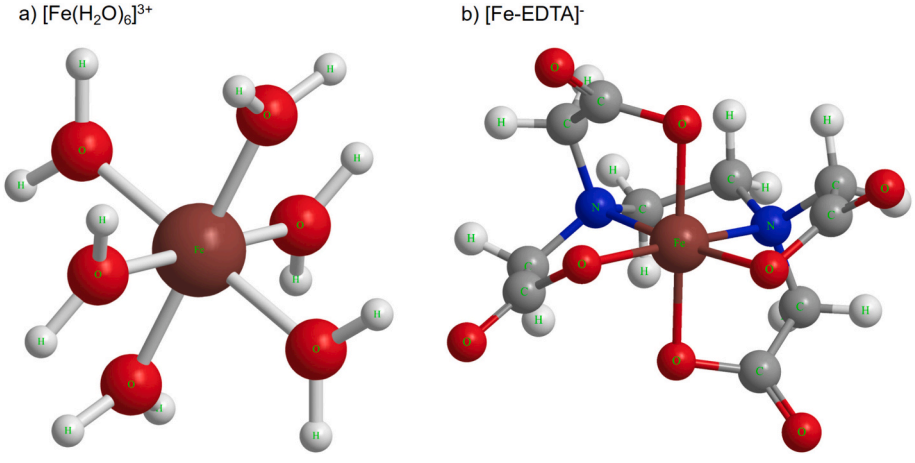

Fig. 12. Fe^{3+} complexes coordinated by H_2O and $EDTA^{4-}$.

QXRD results) of the two most hydraulically reactive phases, brownmillerite and C_2S ($\alpha' + \beta$), between BOF slag activated by Na_4EDTA (this study) and by K_3-citrate [113]. The K_3-citrate study used a sieved BOF slag with a smaller grain size and a lower w/b ratio (0.16), but the molar quantities of both activators are equivalent (3.1×10^{-3} mol/100 g BOF slag), as described in Section 2.2. It is evident that, compared to K_3-citrate, Na_4EDTA has a markedly stronger effect on early hydration, particularly for C_2S, which shows almost double the 7 d hydration degree under Na_4EDTA activation. This substantial difference in early hydration activation can be explained by the considerably higher stability constants (orders of magnitude) of M-EDTA complexes compared to M-Citrate complexes, as shown in Table 5 [36,38,39,109,110,114].

However, the complexation (chelation) reaction is complicated, especially within the BOF slag system, where multiple metal oxides (minerals) coexist. In addition to the varying K_S of different metal ions, other factors affect the complexation reaction between $EDTA^{4-}$ and metal ions, such as the solubility of metal oxides (minerals) themselves, solution pH, and the relative concentration of $EDTA^{4-}$ to various metal ions [41,45,81,112]. Among these, the solubility of metal oxides (minerals) is a primary determining factor. For example, $EDTA^{4-}$ induces limited dissolution of wuestite and significant depletion of brownmillerite, while magnetite is even less affected than wuestite according to the QXRD results. Since $EDTA^{4-}$ generally forms a 1:1 complex with metal ions [41,81,115], 4.8 wt% of Na_4EDTA can theoretically chelate up to 0.7 wt% of Fe (assuming no complexation with other ions), which is considerably less than the Fe content in dissolved wuestite and brownmillerite. This suggests that the chelation power of $EDTA^{4-}$ plays a crucial role in promoting dissolution and hydration without requiring full complexation of all metal atoms.

The pH of the aqueous environment also affects the complexation reaction due to the competition of H^+ for metal cations and OH^- for $EDTA^{4-}$. This competition varies significantly between metals. For instance, for Ca^{2+}, dissociation of $[Ca\text{-}EDTA]^{2-}$ occurs as pH decreases, as shown in Eq. (5), with near-total dissociation below pH 5.5 [112].

$$CaEDTA^{2-} + 2H^+ \rightleftharpoons H_2EDTA^{2-} + Ca^{2+} \quad (5)$$

In the alkaline environment of a hydrated cementitious system, $[Ca\text{-}EDTA]^{2-}$ dissociation is minimal. However, for Fe^{3+}, increased pH prompts $Fe(OH)_3$ precipitation (Eq. (6)), and $[Fe\text{-}EDTA]^-$ almost entirely transfers into free $EDTA^{4-}$ and ferric hydroxide at pH above 12 [112].

$$FeEDTA^- + 3OH^- \rightleftharpoons Fe(OH)_3 + EDTA^{4-} \quad (6)$$

However, despite the tendency for hydrolysis, the relatively high concentration of the $EDTA^{4-}$ (approximately 0.7 M in the E48 sample) may inhibit the complete precipitation of $Fe(OH)_3$ [41,116]. This inference is corroborated by Fe leaching results, which show a considerable amount of leachable (soluble) Fe ($[Fe\text{-}EDTA]^-$ complexes) in the hydrated system. Nonetheless, some $Fe(OH)_3$ may precipitate during the pH increase, leading to the $EDTA^{4-}$ releasing and re-entering the aqueous environment, because according to the above analysis, the amount of $EDTA^{4-}$ addition is far less from reaching a 1:1 ratio with the iron in the dissolved minerals, not to mention that C_2S is also significantly activated simultaneously. That is to say, in this system, (part of) the activator $EDTA^{4-}$ is likely to be recyclable and can continue to play a certain role as the hydration proceeds.

Notably, for the chelated metals ($[M\text{-}EDTA]^{n-}$), the six coordination bonds effectively sequester them, preventing their incorporation into the frameworks of hydration products, such as the hydrogarnet series and C-S-H gel, in the form of M-O polyhedra or interlayer cations. However, according to the FTIR study, some $EDTA^{4-}$ ($[M\text{-}EDTA]^{n-}$ complexes) stay in the matrix of hydration products, particularly at later ages (28 d). These suggest that this fraction of $EDTA^{4-}$ ($[M\text{-}EDTA]^{n-}$ complexes) most likely gets incorporated as interlayer anions within the hydrotalcite, as depicted in Appendix C. The hydrotalcite-$EDTA^{4-}$ ($[M\text{-}EDTA]^{n-}$) LDHs structure comprises brucite-like metal (consisting of Mg, Al, and Fe) hydroxides octahedral layers, interlayer anions (carbonates and $EDTA^{4-}$ ($[M\text{-}EDTA]^{n-}$ complexes)), and water molecules. The incorporation of $EDTA^{4-}$ ($[M\text{-}EDTA]^{n-}$ complexes) into the hydrotalcite interlayer causes the further broadening or even disappearance of the XRD peak of hydrotalcite in the Na_4EDTA-activated samples, as illustrated in the zoomed view of the hydrotalcite diffraction peak in Fig. 3. This may explain why the (rescaled) hydrotalcite content is lower in the Na_4EDTA-activated samples at 7 and 28 d compared to the reference sample as this part of hydrotalcite has become X-ray amorphous.

Based on the above analyses, the general BOF slag hydration equation with the activation of Na_4EDTA can be expressed as Eq. (7) [10,117]. It needs to be noted that magnetite hydration (depletion) is not included here.

$$\begin{matrix} C_2(A,F) + C_2S + RO + H + c \xrightarrow{EDTA^{4-}} \\ CSH + C(A,F)SH + M(A,F)c(EDTA)H \end{matrix} \quad (7)$$

where, $H{=}OH^-$; $c = CO_2$; $C(A,F)SH$ = hydrogarnet, $Ca_3(Al_xFe_{1-x})_2(SiO_4)_y(OH)_{4(3-y)}$; $M(A,F)c(EDTA)H$ = hydrotalcite, $Mg_6Al_{2-i}Fe_i(CO_3)_j(EDTA^{n-})_k(OH)_{(18-2j-nk)}$.

Table 5
(Standard) stability constant of $EDTA^{4-}$ and $citrate^{3-}$ with common metal ions in BOF slag (Log K_S, Eq. (4)).

Ligand (ions)	Ca^{2+}	Fe^{3+}	Mg^{2+}	Al^{3+}
$EDTA^{4-}$	10.7	25.1	8.7	16.1
$Citrate^{3-}$	3.5	11.4	3.5	8.0

4. Conclusion

Na_4EDTA is first proposed as an activator of BOF slag hydration in this research. The effects of its doses on BOF slag phase composition evolution, early hydration kinetics, and microstructural and mechanical properties were studied systematically. The leaching characteristics of Na_4EDTA-activated BOF slag were also examined via a one-stage batch leaching test and ICP-AES analysis. Additionally, the chelation mechanism of $EDTA^{4-}$, underlying its hydration-activation effects, was explored. Based on the investigations and discussion, the following conclusions can be drawn:

- Na_4EDTA significantly enhances BOF slag dissolution and hydration, with no apparent induction period in the Na_4EDTA-activated samples. At higher Na_4EDTA doses, brownmillerite hydration proceeds quickly, completing in a day. The hydration of C_2S is also enhanced when applying Na_4EDTA, particularly at an early age, at high Na_4EDTA doses, though with a lower reactivity than brownmillerite, likely due to the lower affinity of $EDTA^{4-}$ for Ca than Fe.
- The primary crystalline hydration products of BOF slag are hydrogarnet and hydrotalcite. Na_4EDTA significantly promotes the formation of hydrogarnet at all ages while depressing the hydrotalcite generation at 7 and 28 d.
- Na_4EDTA significantly reduces total porosity (from 33.1 % in E00 to 14.9 % in E48 at 28 d), refines pore size distribution, and enhances compressive strength (from 8.6 MPa in E00 to 38.8 MPa in E48 at 28 d) of the stand-alone BOF slag binder. These effects generally increase with Na_4EDTA dosage.
- Despite increased Cr and V leaching in Na_4EDTA-activated samples, all hydrated BOF slag samples exhibit leaching below the Dutch legislative limit. This outcome is attributed to the immobilization capacity of the hydration products.
- With ongoing hydration, $EDTA^{4-}$ ($[M\text{-}EDTA]^{n-}$ complexes) increasingly integrate into the hydration products, with the hydrotalcite (LDHs) most likely serving as the host.

Overall, Na_4EDTA transforms BOF slag from a poorly hydraulically reactive material to a high-performance stand-alone cementitious binder. However, details warrant further exploration. Identifying the optimal Na_4EDTA dosage to balance performance and cost is critical for practical applications. Additionally, regulation of the setting and hardening time of the Na_4EDTA-activated BOF slag binder by incorporating additives such as gypsum is necessary for future applications. Currently, there is no unified understanding of the specific adsorption/desorption processes of $EDTA^{4-}$ and corresponding dissolution-promoting effects, particularly in systems with several different mineral phases. A systematic comparative study of Na_4EDTA and other chelators could also help understand the reactions better.

CRediT authorship contribution statement

Zhihan Jiang: Formal analysis, Data curation, Conceptualization, Writing – original draft, Methodology, Investigation. **Xuan Ling:** Writing – review & editing, Methodology, Investigation, Data curation. **Quan Liu:** Writing – original draft, Investigation, Data curation. **Helong Song:** Writing – review & editing, Data curation. **Katrin Schollbach:** Writing – review & editing, Supervision, Conceptualization. **H.J.H. Brouwers:** Writing – review & editing, Supervision.

Declaration of competing interest

The authors declare that they have no known competing financial interests or personal relationships that could have appeared to influence the work reported in this paper.

Acknowledgment

This work was supported by the China Scholarship Council (fund No. 202006950032). We express our sincere gratitude to Anneke Delsing for the help in the ICP-AES analysis. We would also like to thank Tata Steel (The Netherlands) for offering the raw BOF slag.

Appendix A. Quantitative mineralogical compositions of raw and hydrated BOF slag retrieved by Rietveld refinement (wt%)

Phase	Raw BOF	1 d				7 d				28 d			
		E00	E12	E24	E48	E00	E12	E24	E48	E00	E12	E24	E48
Wuestite	21.9	21.4	19.2	16.4	15.3	20.9	15.0	14.8	14.2	19.4	16.7	14.9	15.7
Magnetite	4.9	5.0	4.3	4.6	3.9	5.1	4.3	3.8	4.0	5.0	4.2	3.8	3.9
Brownmillerite	13.0	12.0	6.9	5.8	3.8	11.1	5.7	5.6	4.3	11.2	5.2	4.0	3.8
C_2S ($\alpha' + \beta$)	35.4	34.9	31.8	29.8	26.3	32.1	28.9	26.5	26.4	29.7	26.4	25.4	22.9
Hydrogarnet	0.0	1.6	5.2	9.5	9.2	2.4	8.4	9.8	12.1	3.0	9.2	12.2	12.6
Hydrotalcite	0.0	2.0	2.9	4.4	3.9	3.3	3.1	2.3	2.9	3.5	2.7	3.3	3.7
Lime	0.7	0.1	0.3	0.2	0.4	0.1	0.1	0.6	0.3	0.2	0.3	0.3	0.1
Portlandite	0.2	0.1	0.1	0.2	0.4	0.7	0.1	0.3	0.7	1.2	0.4	1.0	0.8
Calcite	0.3	0.3	0.5	1.0	0.6	0.5	0.6	0.8	0.9	0.9	1.0	0.9	1.1
Amorphous	23.6	22.6	28.8	28.1	36.2	23.8	33.8	35.5	34.2	25.9	33.9	34.2	35.4
GOF	1.8	1.7	1.8	1.6	1.8	1.7	1.8	1.8	1.7	1.6	1.5	1.8	1.7
Rwp (%)	3.6	3.2	2.6	3.1	3.0	3.5	3.7	2.6	3.6	3.5	2.8	3.4	3.5

Appendix B. Calculated XRD patterns (obtained through Rietveld refinement fitting) v.s. Observed XRD patterns. (Blue: tested; red: calculated; gray: difference)

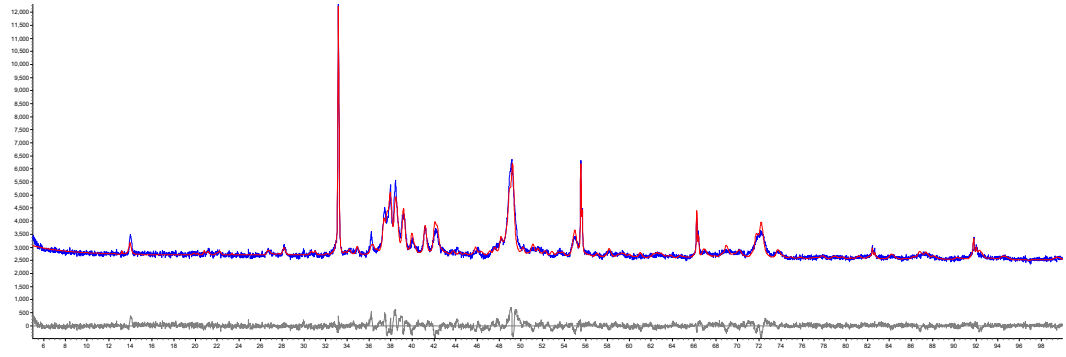

Appendix B.1. Raw BOF slag.

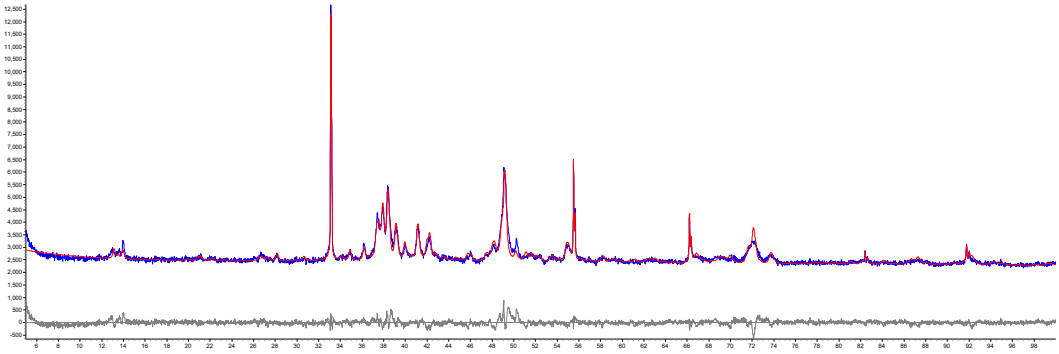

Appendix B.2. 1d E00.

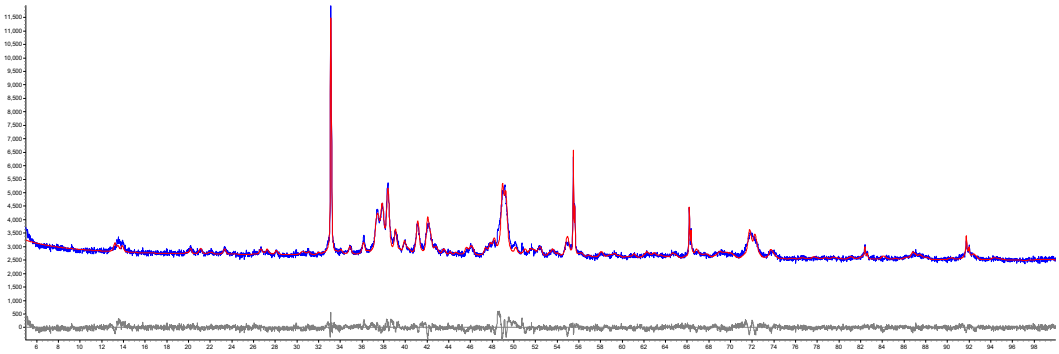

Appendix B.3. 1d E12.

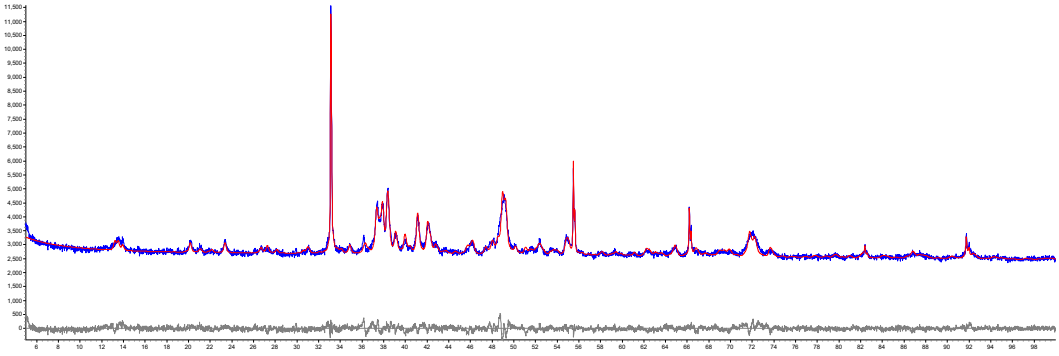

Appendix B.4. 1d E24.

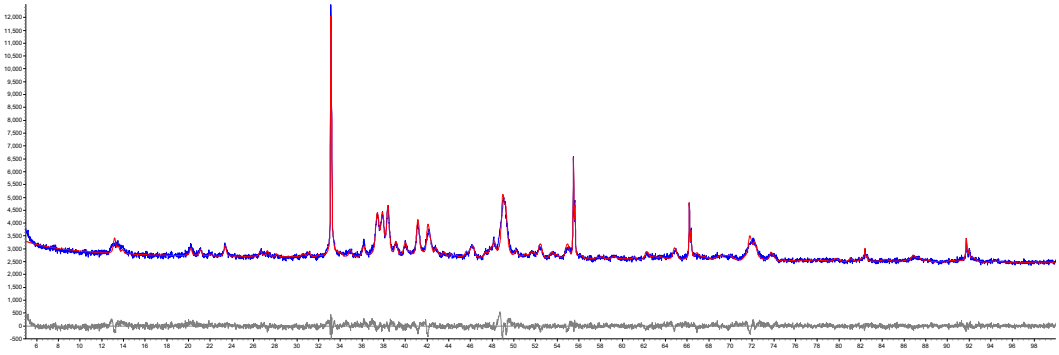

Appendix B.5. 1d E48.

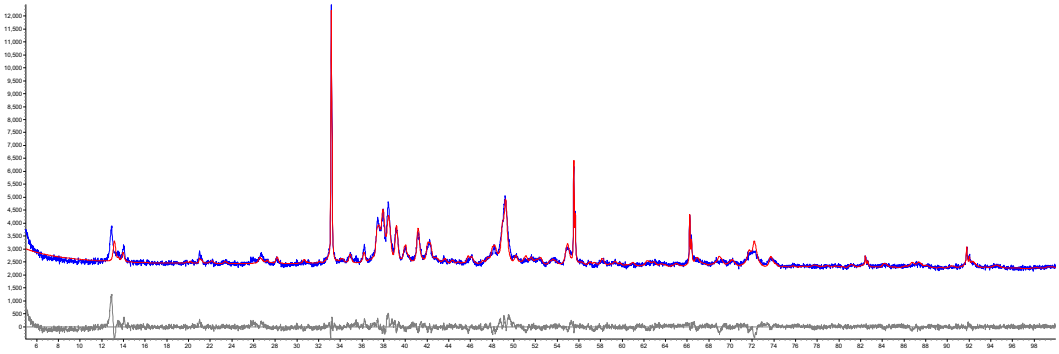

Appendix B.6. 7d E00.

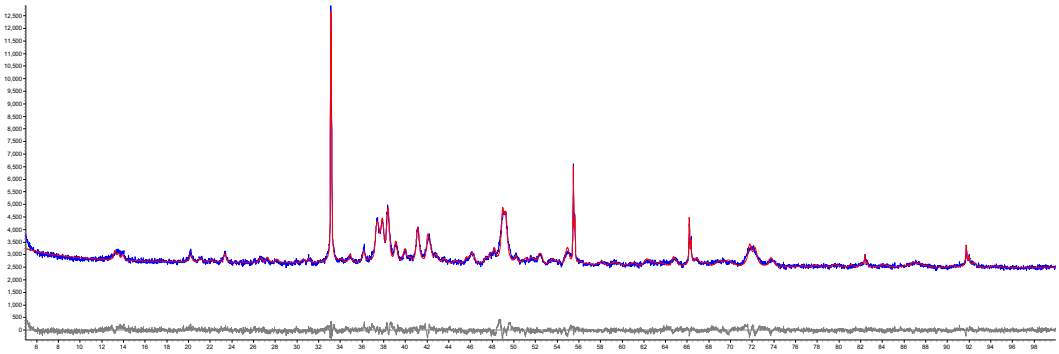

Appendix B.7. 7d E12.

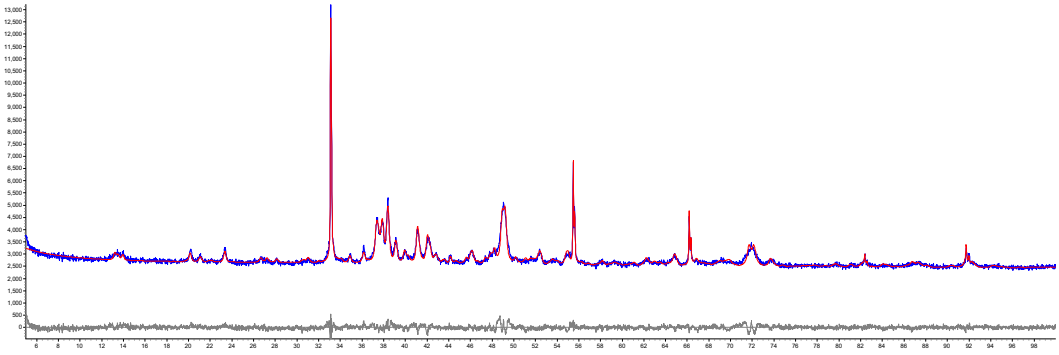

Appendix B.8. 7d E24.

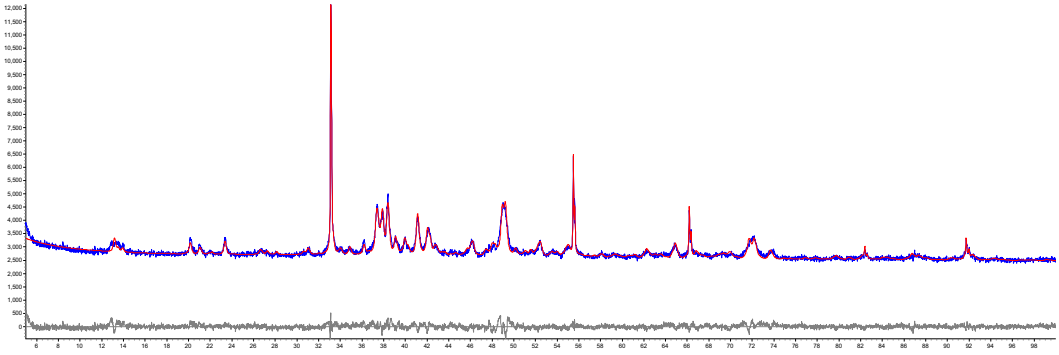

Appendix B.9. 7d E48.

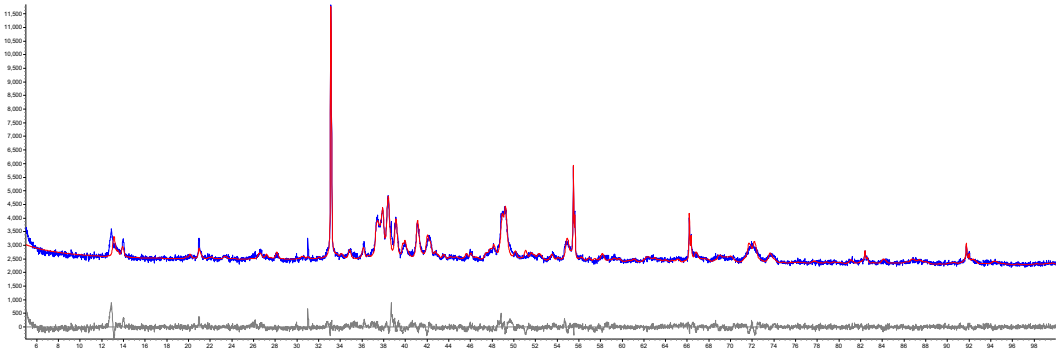

Appendix B.10. 28d E00.

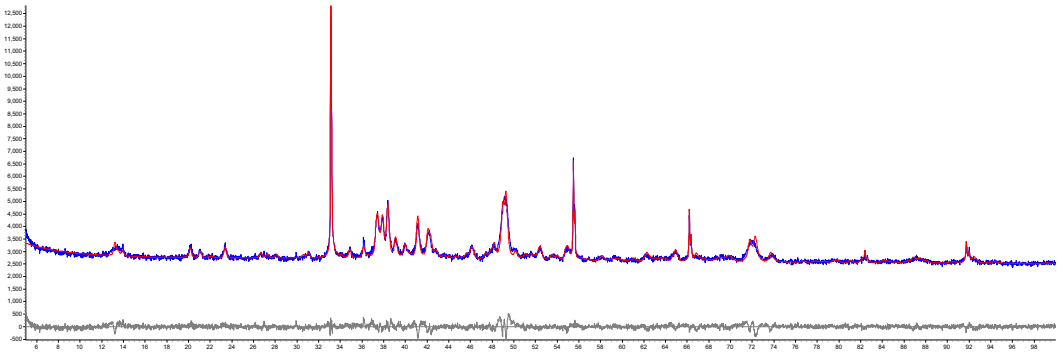

Appendix B.11. 28d E12.

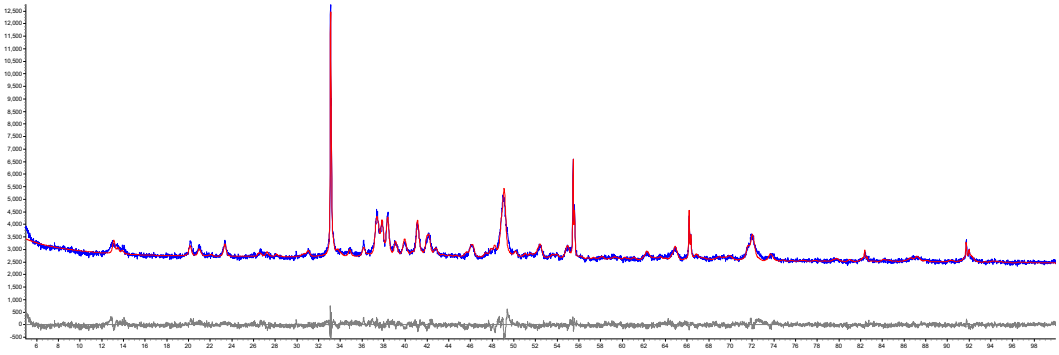

Appendix B.12. 28d E24.

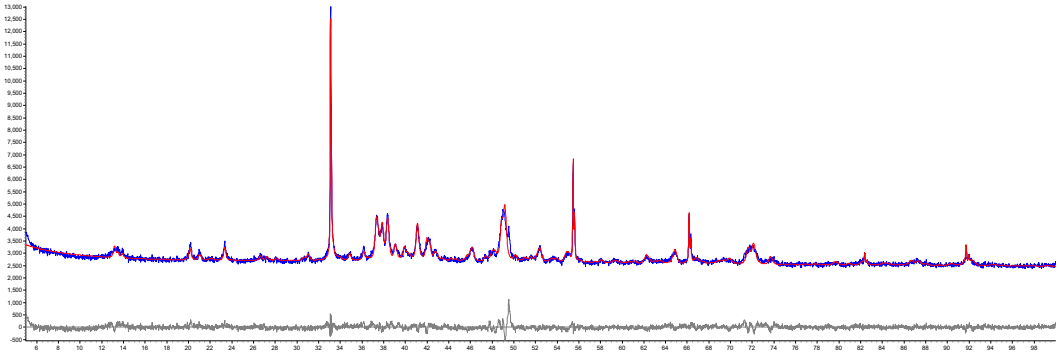

Appendix B.13. 28d E48.

Appendix C. A schematic diagram of EDTA-incorporated hydrotalcite LDHs structure

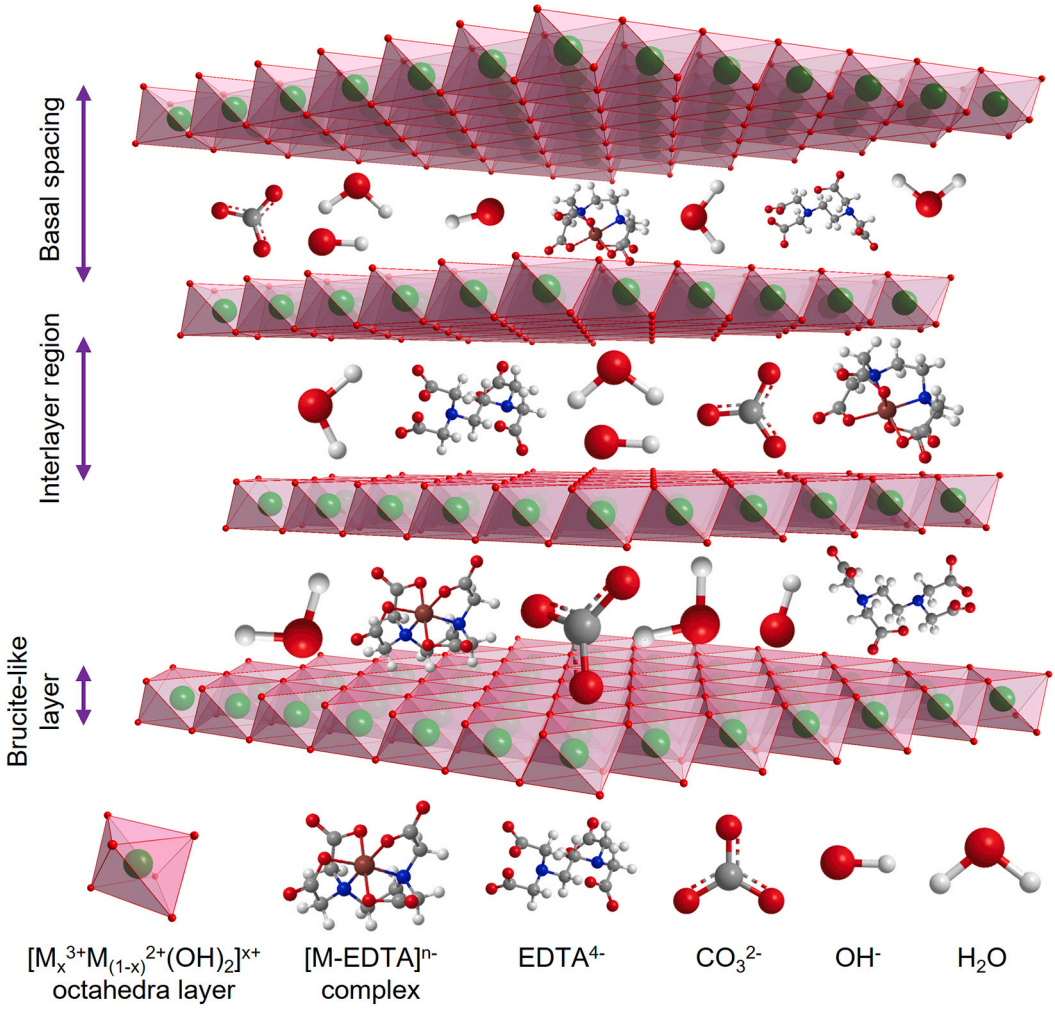

Data availability

Data will be made available on request.

References

[1] S.K. Singh, P. Rekha, M. Surya, Utilization of Linz–Donawitz slag from steel industry for waste minimization, J. Mater. Cycles Waste Manag. 22 (2020) 611–627, https://doi.org/10.1007/s10163-020-00981-z.
[2] Y. Jiang, T.C. Ling, C. Shi, S.Y. Pan, Characteristics of steel slags and their use in cement and concrete—a review, Resour. Conserv. Recycl. 136 (2018) 187–197, https://doi.org/10.1016/j.resconrec.2018.04.023.
[3] M. Díaz-Piloneta, F. Ortega-Fernández, M. Terrados-Cristos, J.V. Álvarez-Cabal, Application of steel slag for degraded land remediation, Land 11 (2) (2022) 224, https://doi.org/10.3390/LAND11020224.
[4] K. Schollbach, S. van der Laan, Microstructure analysis with quantitative phase mapping using SEM-EDS and phase recognition and characterization (PARC) software: applied to steelmaking slag, Ind. Waste Charact. Modif. Appl. Residues (2022) 57–96, https://doi.org/10.1515/9783110674941-003.
[5] E. Belhadj, C. Diliberto, A. Lecomte, Characterization and activation of basic oxygen furnace slag, Cem. Concr. Compos. 34 (2012) 34–40, https://doi.org/10.1016/j.cemconcomp.2011.08.012.
[6] Q. Wang, P. Yan, J. Yang, B. Zhang, Influence of steel slag on mechanical properties and durability of concrete, Constr. Build. Mater. 47 (2013) 1414–1420, https://doi.org/10.1016/J.CONBUILDMAT.2013.06.044.
[7] A.M. Rashad, A synopsis manual about recycling steel slag as a cementitious material, J. Mater. Res. Technol. 8 (2019) 4940–4955, https://doi.org/10.1016/j.jmrt.2019.06.038.
[8] A.M. Kaja, K. Schollbach, S. Melzer, S.R. van der Laan, H.J.H. Brouwers, Q. Yu, Hydration of potassium citrate-activated BOF slag, Cem. Concr. Res. 140 (2021) 106291, https://doi.org/10.1016/j.cemconres.2020.106291.
[9] Z. Jiang, J. Zepper, X. Ling, K. Schollbach, H.J.H. Brouwers, Potassium citrate-activated pure BOF slag-based mortars utilizing carbonated and autoclaved BOF slag aggregates, Cem. Concr. Compos. 150 (2024) 105564, https://doi.org/10.1016/j.cemconcomp.2024.105564.
[10] W.F. Santos, K. Schollbach, S. Melzer, S.R. van der Laan, H.J.H. Brouwers, Quantitative analysis and phase assemblage of basic oxygen furnace slag hydration, J. Hazard. Mater. 450 (2023) 131029, https://doi.org/10.1016/j.jhazmat.2023.131029.
[11] W. Franco Santos, J.J. Botterweg, S. Chaves Figueiredo, K. Schollbach, S. van der Laan, H.J.H. Brouwers, Sodium oxalate activation of basic oxygen furnace slag for building materials, Resour. Conserv. Recycl. 198 (2023) 107174, https://doi.org/10.1016/j.resconrec.2023.107174.
[12] A. van Zomeren, S.R. van der Laan, H.B.A. Kobesen, W.J.J. Huijgen, R.N. J. Comans, Changes in mineralogical and leaching properties of converter steel slag resulting from accelerated carbonation at low CO2 pressure, Waste Manag. 31 (2011) 2236–2244, https://doi.org/10.1016/J.WASMAN.2011.05.022.
[13] M.J. Ahmed, R. Cuijpers, K. Schollbach, S. Van Der Laan, M. Van Wijngaarden-Kroft, T. Verhoeven, H.J.H. Brouwers, V and Cr substitution in dicalcium silicate under oxidizing and reducing conditions – synthesis, reactivity, and leaching behavior studies, J. Hazard. Mater. 442 (2023) 130032, https://doi.org/10.1016/J.JHAZMAT.2022.130032.
[14] L. Chang, H. Liu, J. Wang, L. Song, Y. Wang, S. Cui, Effect of chelation via ethanol-diisopropanolamine on hydration of pure steel slag, Construct. Build Mater. 357 (2022) 129372, https://doi.org/10.1016/j.conbuildmat.2022.129372.

[15] U.C. Mishra, S. Sarsaiya, A. Gupta, A systematic review on the impact of cement industries on the natural environment, Environ. Sci. Pollut. Res. 29 (2022) 18440–18451, https://doi.org/10.1007/S11356-022-18672-7. /FIGURES/4.

[16] Q. Wang, P. Yan, Hydration properties of basic oxygen furnace steel slag, Constr. Build. Mater. 24 (2010) 1134–1140, https://doi.org/10.1016/j.conbuildmat.2009.12.028.

[17] Q. Wang, J. Yang, P. Yan, Cementitious properties of super-fine steel slag, Powder Technol. 245 (2013) 35–39, https://doi.org/10.1016/j.powtec.2013.04.016.

[18] J.C.O. Zepper, S.R. van der Laan, K. Schollbach, H.J.H. Brouwers, Reactivity of BOF slag under autoclaving conditions, Constr. Build. Mater. 364 (2023) 129957, https://doi.org/10.1016/j.conbuildmat.2022.129957.

[19] X. Guo, H. Shi, Modification of steel slag powder by mineral admixture and chemical activators to utilize in cement-based materials, Mater. Struct. 46 (2013) 1265–1273, https://doi.org/10.1617/S11527-012-9970-7.

[20] T. Zhang, Q. Yu, J. Wei, J. Li, Investigation on mechanical properties, durability and micro-structural development of steel slag blended cements, J. Therm. Anal. Calorim. 110 (2012) 633–639, https://doi.org/10.1007/s10973-011-1853-6.

[21] S. Smillie, F.P. Glasser, Reaction of EDTA, oxalic acid and citric acid with Portland cement, Adv. Cem. Res. 11 (1999) 97–101, https://doi.org/10.1680/adcr.1999.11.2.97.

[22] A.S. Reddy, R.K. Pradhan, S. Chandra, Utilization of Basic Oxygen Furnace (BOF) slag in the production of a hydraulic cement binder, Int. J. Miner. Process. 79 (2006) 98–105, https://doi.org/10.1016/J.MINPRO.2006.01.001.

[23] S. Liu, L. Li, Influence of fineness on the cementitious properties of steel slag, J. Therm. Anal. Calorim. 117 (2014) 629–634, https://doi.org/10.1007/S10973-014-3789-0. /FIGURES/10.

[24] A. Duda, Hydraulic reactions of LD steelwork slags, Cem. Concr. Res. 19 (1989) 793–801, https://doi.org/10.1016/0008-8846(89)90050-1.

[25] T.S. Zhang, F.T. Liu, S.Q. Liu, Z.H. Zhou, X. Cheng, Factors influencing the properties of a steel slag composite cement, Adv. Cem. Res. 20 (4) (2008) 145–150, https://doi.org/10.1680/ADCR.2008.20.4.145.

[26] S. Kourounis, S. Tsivilis, P.E. Tsakiridis, G.D. Papadimitriou, Z. Tsibouki, Properties and hydration of blended cements with steelmaking slag, Cem. Concr. Res. 37 (2007) 815–822, https://doi.org/10.1016/j.cemconres.2007.03.008.

[27] Y.M. Kim, S.H. Hong, Influence of minor ions on the stability and hydration rates of β-dicalcium silicate, J. Am. Ceram. Soc. 87 (2004) 900–905, https://doi.org/10.1111/j.1551-2916.2004.00900.x.

[28] B.Z. Dilnesa, E. Wieland, B. Lothenbach, R. Dähn, K.L. Scrivener, Fe-containing phases in hydrated cements, Cem. Concr. Res. 58 (2014) 45–55, https://doi.org/10.1016/j.cemconres.2013.12.012.

[29] B.Z. Dilnesa, B. Lothenbach, G. Renaudin, A. Wichser, D. Kulik, Synthesis and characterization of hydrogarnet Ca3(AlxFe1 − x)2(SiO4)y(OH)4(3 − y), Cem. Concr. Res. 59 (2014) 96–111, https://doi.org/10.1016/J.CEMCONRES.2014.02.001.

[30] M.L. Peter, C. Hewlett, Lea's Chemistry of Cement and Concrete, 5 th, Mathew Deans, 2019.

[31] A.M. Kaja, S. Melzer, H.J.H. Brouwers, Q. Yu, On the optimization of BOF slag hydration kinetics, Cem. Concr. Compos. 124 (2021) 104262, https://doi.org/10.1016/j.cemconcomp.2021.104262.

[32] R. Sun, P. Shen, D. Wang, J. Wang, Z. Liu, K. Fang, Enhancing hydration of steel slag-based composite cementitious material: synergistic effect of triisopropanolamine (TIPA) and sulfite/sulfate, Cem. Concr. Res. 184 (2024) 107619, https://doi.org/10.1016/J.CEMCONRES.2024.107619.

[33] S. Yang, J. Wang, S. Cui, H. Liu, X. Wang, Impact of four kinds of alkanolamines on hydration of steel slag-blended cementitious materials, Constr. Build. Mater. 131 (2017) 655–666, https://doi.org/10.1016/J.CONBUILDMAT.2016.09.060.

[34] J. Wang, L. Chang, D. Yue, Y. Zhou, H. Liu, Y. Wang, S. Yang, S. Cui, Effect of chelating solubilization via different alkanolamines on the dissolution properties of steel slag, J. Clean. Prod. 365 (2022) 132824, https://doi.org/10.1016/j.jclepro.2022.132824.

[35] R. Smith, A. Martell, Inorganic Complexes, 1976.

[36] R.M. Smith, A.E. Martell, Second Supplement, 1976, https://doi.org/10.1007/978-1-4757-5506-0.

[37] A.E. Martell, R.M. Smith, Amines, 1976.

[38] A.E. Martell, R.M. Smith, First Supplement, 1982, https://doi.org/10.1007/978-1-4615-6761-5.

[39] R.M. Smith, A.E. Martell, Other Organic Ligands, 1976, https://doi.org/10.1007/978-1-4757-1568-2.

[40] J.R. Hart, Ullmann's Encyclopedia of Industrial Chemistry, Wiley-VCH, Weinheim, 2000, https://doi.org/10.1002/14356007.a10_095.

[41] M. Mosher, P. Kelter, Coordination Complexes, an Introd. Chem, 2023, pp. 903–937, https://doi.org/10.1007/978-3-030-90267-4_19.

[42] H. Foreman, M. Vier, M. Magee, The metabolism of C14-labeled ethylenediaminetetraacetic acid in the rat, J. Biol. Chem. 203 (1953) 1045–1053, https://doi.org/10.1016/S0021-9258(19)52375-4.

[43] M.A. Zaitoun, C.T. Lin, Chelating behavior between metal ions and EDTA in sol - gel matrix, J. Phys. Chem. B 101 (1997) 1857–1860, https://doi.org/10.1021/jp963102d.

[44] A. Fulgenzi, M.E. Ferrero, EDTA chelation therapy for the treatment of neurotoxicity, Int. J. Mol. Sci. 20 (2019), https://doi.org/10.3390/IJMS20051019.

[45] S.J.S. Flora, V. Pachauri, Chelation in metal intoxication, Int. J. Environ. Res. Public Health 7 (2010) 2745–2788, https://doi.org/10.3390/ijerph7072745.

[46] L. Chi, W. Li, Z. Li, Z. Wang, S. Lu, Q. Liu, Investigation of the hydration properties of cement with EDTA by alternative current impedance spectroscopy, Cem. Concr. Compos. 126 (2022) 104365, https://doi.org/10.1016/j.cemconcomp.2021.104365.

[47] K. Gu, Y. Maierdan, B. Chen, Effects of ethylenediamine tetra-acetic acid (EDTA) and its disodium salt derivative (EDTA-Na) on the characteristics of magnesium oxysulfate (MOS) cement, Compos. Part B Eng. 232 (2022) 109654, https://doi.org/10.1016/J.COMPOSITESB.2022.109654.

[48] J. Wang, Y. Wang, H. Liu, L. Chang, H. Wang, Y. Wang, S. Cui, Effect of disodium EDTA on hydration and mechanical properties of calcium sulphoaluminate-belite cement, Cem. Concr. Res. 164 (2023) 107041, https://doi.org/10.1016/J.CEMCONRES.2022.107041.

[49] F. Scholz, H. Kahlert, Chemical Equilibria in Analytical Chemistry: The Theory of Acid–Base, Complex, Precipitation and Redox Equilibria, 1st ed., Springer International Publishing, 2019 https://doi.org/10.1007/978-3-030-17180-3.

[50] K. Zhang, Z. Dai, W. Zhang, Q. Gao, Y. Dai, F. Xia, X. Zhang, EDTA-based adsorbents for the removal of metal ions in wastewater, Coord. Chem. Rev. 434 (2021) 213809, https://doi.org/10.1016/J.CCR.2021.213809.

[51] J. Ma, G. Zhou, L. Chu, Y. Liu, C. Liu, S. Luo, Y. Wei, Efficient removal of heavy metal ions with an EDTA functionalized chitosan/polyacrylamide double network hydrogel, ACS Sustain. Chem. Eng. 5 (1) (2017) 843–851, https://doi.org/10.1021/ACSSUSCHEMENG.6B02181.

[52] J.R. Hart, Ethylenediaminetetraacetic acid and related chelating agents, in: Ullmann's Encycl. Ind. Chem, John Wiley & Sons, Ltd, 2011, https://doi.org/10.1002/14356007.a10_095.pub2.

[53] British Standards Institution BSI, Methods of Testing Cement Part 1: Determination of Strength, 2016.

[54] W. Wong-Ng, C.R. Hubbard, Standard reference materials for X-ray diffraction part II. Calibration using d-spacing standards, Powder Diffr. 2 (1987) 242–248, https://doi.org/10.1017/S0885715600012884.

[55] K. Scrivener, R. Snellings, B. Lothenbach, A Practical Guide to Microstructural Analysis of Cementitious Materials, CRC Press, 2016, https://doi.org/10.1201/B19074.

[56] British Standards Institution., Methods of Testing Cement. Part 1, Determination of Strength., (n.d.) 33. https://www.en-standard.eu/bs-en-196-1-2016-methods-of-testing-cement-determination-of-strength/ (accessed July 25, 2023).

[57] N. Hearn, R.D. Hooton, Sample mass and dimension effects on mercury intrusion porosimetry results, Cem. Concr. Res. 22 (1992) 970–980, https://doi.org/10.1016/0008-8846(92)90121-B.

[58] F. Moro, H. Böhni, Ink-bottle effect in mercury intrusion porosimetry of cement-based materials, J. Colloid Interface Sci. 246 (2002) 135–149, https://doi.org/10.1006/JCIS.2001.7962.

[59] European Committee for Standardizaiton, EN 12457–2, characterisation of waste. Leaching. Compliance test for leaching of granular waste materials and sludges, 2014.

[60] B.H. Toby, R factors in Rietveld analysis: how good is good enough? Powder Diffr. 21 (2006) 67–70, https://doi.org/10.1154/1.2179804.

[61] C. Thomas, J. Rosales, J.A. Polanco, F. Agrela, Steel slags, new trends eco-efficient, Recycl. Concr. (2019) 169–190, https://doi.org/10.1016/B978-0-08-102480-5.00007-5.

[62] A.W. Weeber, H. Bakker, Amorphization by ball milling. A review, Phys. B Condens. Matter 153 (1988) 93–135, https://doi.org/10.1016/0921-4526(88)90038-5.

[63] C. van Hoek, J. Small, S. van der Laan, Large-area phase mapping using P h A se R ecognition and C haracterization (PARC) software, Micros. Today. 24 (2016) 12–21, https://doi.org/10.1017/s1551929516000572.

[64] J. Astoveza, R. Trauchessec, R. Soth, Y. Pontikes, Properties of calcium aluminate blended cement incorporating iron-rich slag: evolution over a curing period of 1 year, Constr. Build. Mater. 282 (2021) 122569.

[65] K. Rozov, U. Berner, C. Taviot-Gueho, F. Leroux, G. Renaudin, D. Kulik, L. W. Diamond, Synthesis and characterization of the LDH hydrotalcite–pyroaurite solid-solution series, Cem. Concr. Res. 40 (2010) 1248–1254, https://doi.org/10.1016/J.CEMCONRES.2009.08.031.

[66] C.A. Geiger, G.R. Rossman, Micro- and nano-size hydrogarnet clusters and proton ordering in calcium silicate garnet: Part I. The quest to understand the nature of "water" in garnet continues, Am. Mineral. 105 (2020) 455–467, https://doi.org/10.2138/AM-2020-7256. /ASSET/GRAPHIC/J_AM-2020-7256_FIG_012.JPG.

[67] A. Cuesta, A. Ayuela, M.A.G. Aranda, Belite cements and their activation, Cem. Concr. Res. 140 (2021) 106319, https://doi.org/10.1016/j.cemconres.2020.106319.

[68] K. Noréan, J.S. Loring, J.R. Bargar, P. Persson, Adsorption mechanisms of EDTA at the water-iron oxide interface: implications for dissolution, J. Phys. Chem. C 113 (2009) 7762–7771, https://doi.org/10.1021/jp809190m.

[69] C. Nalet, A. Nonat, Ionic complexation and adsorption of small organic molecules on calcium silicate hydrate: relation with their retarding effect on the hydration of C3S, Cem. Concr. Res. 89 (2016) 97–108, https://doi.org/10.1016/j.cemconres.2016.08.012.

[70] G.R. Qian, D.D. Sun, J.H. Tay, Z.Y. Lai, Hydrothermal reaction and autoclave stability of Mg bearing RO phase in steel slag, Br. Ceram. Trans. 101 (2002) 159–164, https://doi.org/10.1179/096797802225003415.

[71] I. Strandkvist, Å. Sandström, F. Engström, Effect of FeO/MgO ratio on dissolution and leaching of magnesiowüstite, Steel Res. Int. 88 (2017) 1600322, https://doi.org/10.1002/SRIN.201600322.

[72] L. De Windt, P. Chaurand, J. Rose, Kinetics of steel slag leaching: batch tests and modeling, Waste Manag. 31 (2011) 225–235, https://doi.org/10.1016/J.WASMAN.2010.05.018.

[73] M.A. Tayeb, A.N. Assis, S. Sridhar, R.J. Fruehan, Mgo solubility in steelmaking slags, Metall. Mater. Trans. B, Process Metall. Mater. Sci. 46 (2015) 1112–1114, https://doi.org/10.1007/S11663-015-0352-8. /FIGURES/4.

[74] Š. Hošková, P. Tichá, P. Demo, Determination of calcium ions in hydrated cement paste at early stage, Mater. Sci. Forum 636–637 (2010) 1239–1243, https://doi.org/10.4028/WWW.SCIENTIFIC.NET/MSF.636-637.1239.

[75] N. Vogler, P. Drabetzki, M. Lindemann, H.C. Kühne, Description of the concrete carbonation process with adjusted depth-resolved thermogravimetric analysis, J. Therm. Anal. Calorim. 147 (2022) 6167–6180, https://doi.org/10.1007/S10973-021-10966-1/TABLES/2.

[76] M. Zajac, S.K. Bremseth, M. Whitehead, M. Ben Haha, Effect of CaMg(CO3)2 on hydrate assemblages and mechanical properties of hydrated cement pastes at 40 °C and 60 °C, Cem. Concr. Res. 65 (2014) 21–29, https://doi.org/10.1016/J.CEMCONRES.2014.07.002.

[77] W. Kurdowski, Cement and Concrete Chemistry, Springer Netherlands, Dordrecht, 2014, https://doi.org/10.1007/978-94-007-7945-7.

[78] I. Galan, F.P. Glasser, C. Andrade, Calcium carbonate decomposition, J. Therm. Anal. Calorim. 111 (2013) 1197–1202, https://doi.org/10.1007/S10973-012-2290-X/FIGURES/12.

[79] Y.A. Villagrán-Zaccardi, H. Egüez-Alava, K. De Buysser, E. Gruyaert, N. De Belie, Calibrated quantitative thermogravimetric analysis for the determination of portlandite and calcite content in hydrated cementitious systems, Mater. Struct. Constr. 50 (2017) 1–10, https://doi.org/10.1617/S11527-017-1046-2/TABLES/3.

[80] S.J. Palmer, H.J. Spratt, R.L. Frost, Thermal decomposition of hydrotalcites with variable cationic ratios, J. Therm. Anal. Calorim. 95 (2009) 123–129, https://doi.org/10.1007/S10973-008-8992-4. /METRICS.

[81] B.E. Douglas, D.J. Radanović, Coordination chemistry of hexadentate EDTA-type ligands with M(III) ions, Coord. Chem. Rev. 128 (1993) 139–165, https://doi.org/10.1016/0010-8545(93)80027-3.

[82] S. Tomar, S. Gupta, A. Priyam, B. Bhushan, A. Singh, U.K. Dwivedi, R.K. Choubey, Temporal evolution of optical absorption and emission spectra of thiol capped CdTe quantum dots, Appl. Phys. A Mater. Sci. Process. 128 (2022) 1–13, https://doi.org/10.1007/S00339-022-06087-7/FIGURES/10.

[83] A.C. Gigante, F.J. Caires, D.J.C. Gomes, L.S. Lima, O. Treu-Filho, M. Pivatto, M. Ionashiro, Spectroscopic study and thermal behavior of trivalent lanthanides and yttrium(III) chelates of EDTA using TG-DSC, FTIR, and TG-DSC coupled to FTIR, J. Therm. Anal. Calorim. 115 (2014) 127–135, https://doi.org/10.1007/s10973-013-3284-z.

[84] K.C. Lanigan, K. Pidsosny, Reflectance FTIR spectroscopic analysis of metal complexation to EDTA and EDDS, Vib. Spectrosc. 45 (2007) 2–9, https://doi.org/10.1016/J.VIBSPEC.2007.03.003.

[85] H. Chen, J. Lin, N. Zhang, L. Chen, S. Zhong, Y. Wang, W. Zhang, Q. Ling, Preparation of MgAl-EDTA-LDH based electrospun nanofiber membrane and its adsorption properties of copper(II) from wastewater, J. Hazard. Mater. 345 (2018) 1–9, https://doi.org/10.1016/J.JHAZMAT.2017.11.002.

[86] G. Möschner, B. Lothenbach, R. Figi, R. Kretzschmar, Influence of citric acid on the hydration of Portland cement, Cem. Concr. Res. 39 (2009) 275–282, https://doi.org/10.1016/j.cemconres.2009.01.005.

[87] P. Juilland, A. Kumar, E. Gallucci, R.J. Flatt, K.L. Scrivener, Effect of mixing on the early hydration of alite and OPC systems, Cem. Concr. Res. 42 (2012) 1175–1188, https://doi.org/10.1016/J.CEMCONRES.2011.06.011.

[88] A. Viani, L. Zárybnická, R. Ševčík, P. Mácová, J. Machotová, Mechanisms of controlled crystallization of struvite-K by NTA and EDTA sodium salts, J. Cryst. Growth 623 (2023) 127414, https://doi.org/10.1016/J.JCRYSGRO.2023.127414.

[89] J. Prywer, M. Olszynski, Influence of disodium EDTA on the nucleation and growth of struvite and carbonate apatite, J. Cryst. Growth 375 (2013) 108–114, https://doi.org/10.1016/j.jcrysgro.2013.04.027.

[90] T.D. Perry IV, O.W. Duckworth, T.A. Kendall, S.T. Martin, R. Mitchell, Chelating ligand alters the microscopic mechanism of mineral dissolution, J. Am. Chem. Soc. 127 (2005) 5744–5745, https://doi.org/10.1021/ja042737k.

[91] N. Li, C. Shi, Z. Zhang, Understanding the roles of activators towards setting and hardening control of alkali-activated slag cement, Compos. Part B Eng. 171 (2019) 34–45, https://doi.org/10.1016/j.compositesb.2019.04.024.

[92] Q. Zeng, K. Li, T. Fen-Chong, P. Dangla, Pore structure characterization of cement pastes blended with high-volume fly-ash, Cem. Concr. Res. 42 (2012) 194–204, https://doi.org/10.1016/J.CEMCONRES.2011.09.012.

[93] P. Chaurand, J. Rose, J. Domas, J.Y. Bottero, Speciation of Cr and V within BOF steel slag reused in road constructions, J. Geochem. Explor. 88 (2006) 10–14, https://doi.org/10.1016/j.gexplo.2005.08.006.

[94] P. Chaurand, J. Rose, O. Proux, J.L. Hazemann, V. Briois, M. Salome, J. Susini, J. H. Ferrasse, D. Borschneck, J.Y. Bottero, Environmental impact of steel slag reused as aggregates in road manufacturing: molecular mechanisms of chromium and vanadium release, AIP Conf. Proc. 882 (2007) 199–201, https://doi.org/10.1063/1.2644473.

[95] Soil Quality Decree. https://wetten.overheid.nl/BWBR0023085/2015-07-01#BijlageA, 2015.

[96] A.D. Apte, V. Tare, P. Bose, Extent of oxidation of Cr(III) to Cr(VI) under various conditions pertaining to natural environment, J. Hazard. Mater. 128 (2006) 164–174, https://doi.org/10.1016/J.JHAZMAT.2005.07.057.

[97] P. Chaurand, J. Rose, V. Briois, L. Olivi, J.L. Hazemann, O. Proux, J. Domas, J. Y. Bottero, Environmental impacts of steel slag reused in road construction: A crystallographic and molecular (XANES) approach, J. Hazard. Mater. 139 (2007) 537–542, https://doi.org/10.1016/j.jhazmat.2006.02.060.

[98] H. Preßlinger, K.O. Klepp, Vanadium in converter slags, Steel Res. 73 (2002) 522–525, https://doi.org/10.1002/srin.200200022.

[99] P. Chaurand, J. Rose, V. Briois, M. Salome, O. Proux, V. Nassif, L. Olivi, J. Susini, J.L. Hazemann, J.Y. Bottero, New methodological approach for the vanadium K-edge X-ray absorption near-edge structure interpretation: application to the speciation of vanadium in oxide phases from steel slag, J. Phys. Chem. B 111 (2007) 5101–5110, https://doi.org/10.1021/jp063186i.

[100] A. Vollpracht, W. Brameshuber, Binding and leaching of trace elements in Portland cement pastes, Cem. Concr. Res. 79 (2016) 76–92, https://doi.org/10.1016/J.CEMCONRES.2015.08.002.

[101] M.L.D. Gougar, B.E. Scheetz, D.M. Roy, Ettringite and C S H Portland cement phases for waste ion immobilization: a review, Waste Manag. 16 (1996) 295–303, https://doi.org/10.1016/S0956-053X(96)00072-4.

[102] A. Polettini, R. Pomi, P. Sirini, Fractional factorial design to investigate the influence of heavy metals and anions on acid neutralization behavior of cement-based products, Environ. Sci. Technol. 36 (2002) 1584–1591, https://doi.org/10.1021/ES010002Z.

[103] S. Hillier, D.G. Lumsdon, R. Brydson, E. Paterson, Hydrogarnet: a host phase for Cr(VI) in chromite ore processing residue (COPR) and other high pH wastes, Environ. Sci. Technol. 41 (2007) 1921–1927, https://doi.org/10.1021/ES0621997/SUPPL_FILE/ES0621997SI20061220_075011.PDF.

[104] P. Kumarathasan, G.J. McCarthy, D.J. Hassett, D.F. Pflughoeft-Hassett, Oxyanion substituted ettringites: synthesis and characterization; and their potential role in immobilization of As, B, Cr, Se and V, MRS Online Proc. Libr. 1989 178 (2011) 83–104, https://doi.org/10.1557/PROC-178-83, 1781.

[105] M. Ochs, B. Lothenbach, E. Giffaut, Uptake of oxo-anions by cements through solid-solution formation: experimental evidence and modelling, Radiochim. Acta 90 (2002) 639–646, https://doi.org/10.1524/RACT.2002.90.9-11_2002.639/MACHINEREADABLECITATION/RIS.

[106] S.J. Palmer, R.L. Frost, Use of hydrotalcites for the removal of toxic anions from aqueous solutions, Ind. Eng. Chem. Res. 49 (2010) 8969–8976, https://doi.org/10.1021/IE101104R. /ASSET/IMAGES/LARGE/IE-2010-01104R_0007.JPEG.

[107] V. Murthy, H.D. Smith, H. Zhang, S.C. Smith, Molecular modeling of hydrotalcite structure intercalated with transition metal oxide anions: CrO42− and VO43−, J. Phys. Chem. A 115 (2011) 13673–13683, https://doi.org/10.1021/JP2079499. /ASSET/IMAGES/LARGE/JP-2011-079499_0007.JPEG.

[108] G. Crisponi, M. Remelli, Iron chelating agents for the treatment of iron overload, Coord. Chem. Rev. 252 (2008) 1225–1240, https://doi.org/10.1016/j.ccr.2007.12.014.

[109] H.M.N.H. Irving, K. Sharpe, Stabilities of complexes formed by dl- and meso-2,3-diaminobutane-N,N,N′,N′-tetraacetic acid with Fe(II) and with Fe(III), J. Inorg. Nucl. Chem. 33 (1971) 233–243, https://doi.org/10.1016/0022-1902(71)80024-6.

[110] G. Schwarzenbach, R. Gut, G. Anderegg, Komplexone XXV. Die polarographische Untersuchung von Austauschgleichgewichten. Neue Daten der Bildungskonstanten von Metallkomplexen der Äthylendiamin-tetraessigsäure und der 1,2-Diaminocyclohexan-tetraessigsäure, Helv. Chim. Acta 37 (1954) 937–957, https://doi.org/10.1002/HLCA.19540370402.

[111] D. Laboratories CyDTA Table of Stability Constants n.d. https://www.dojindo.eu.com/store/p/736-CyDTA.aspx.

[112] Chelation chemistry, (n.d.). www.dow.com/documents/113/113-01388-01-chelation-chemistry-general-concepts-of-the-chemistry-of-chelation.pdf?iframe=true&.

[113] A.M. Kaja, K. Schollbach, S. Melzer, S.R. van der Laan, H.J.H. Brouwers, Q. Yu, Hydration of potassium citrate-activated BOF slag, Cem. Concr. Res. 140 (2021), https://doi.org/10.1016/j.cemconres.2020.106291.

[114] J.L. Meyer, Formation constants for interaction of citrate with calcium and magnesium lons, Anal. Biochem. 62 (1974) 295–300, https://doi.org/10.1016/0003-2697(74)90391-1.

[115] S. Beck, Fragmentation behavior of EDTA complexes under different activation conditions, J. Mass Spectrom. 56 (2021) e4775, https://doi.org/10.1002/JMS.4775.

[116] B. Nowack, L. Sigg, Dissolution of Fe(III)(hydr) oxides by metal-EDTA complexes, Geochim. Cosmochim. Acta 61 (1997) 951–963, https://doi.org/10.1016/s0016-7037(96)00391-2.

[117] B. Lothenbach, F. Winnefeld, Thermodynamic modelling of the hydration of Portland cement, Cem. Concr. Res. 36 (2006) 209–226, https://doi.org/10.1016/J.CEMCONRES.2005.03.001.